Photovoltaic cells – from the experiment of Bequerel to the dye-sensitized solar cell (DSSC)

Diagram of apparatus described by Becquerel (1839)

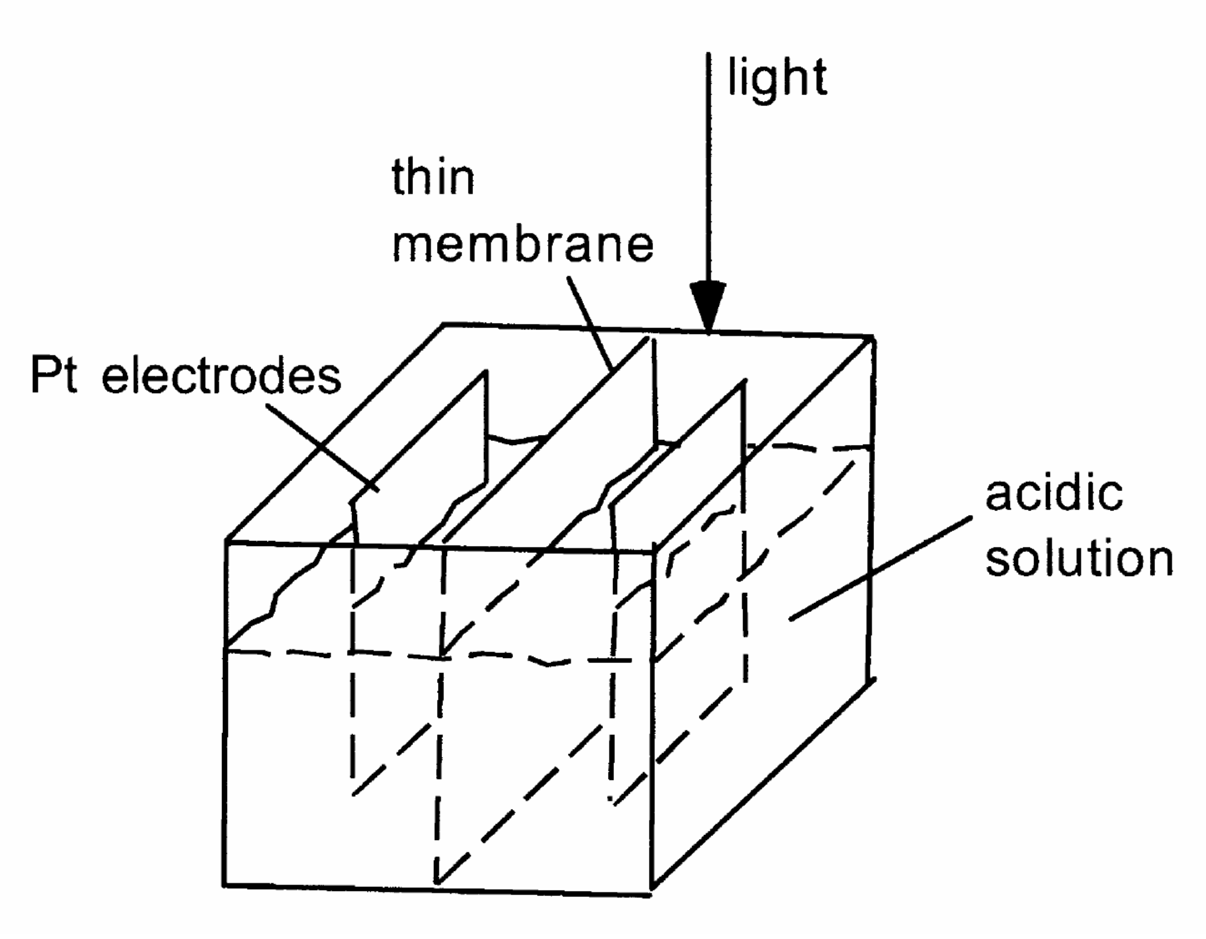

Sample geometry used by Adams and Day (1876) for the investigation of the photovoltaic effect in selenium

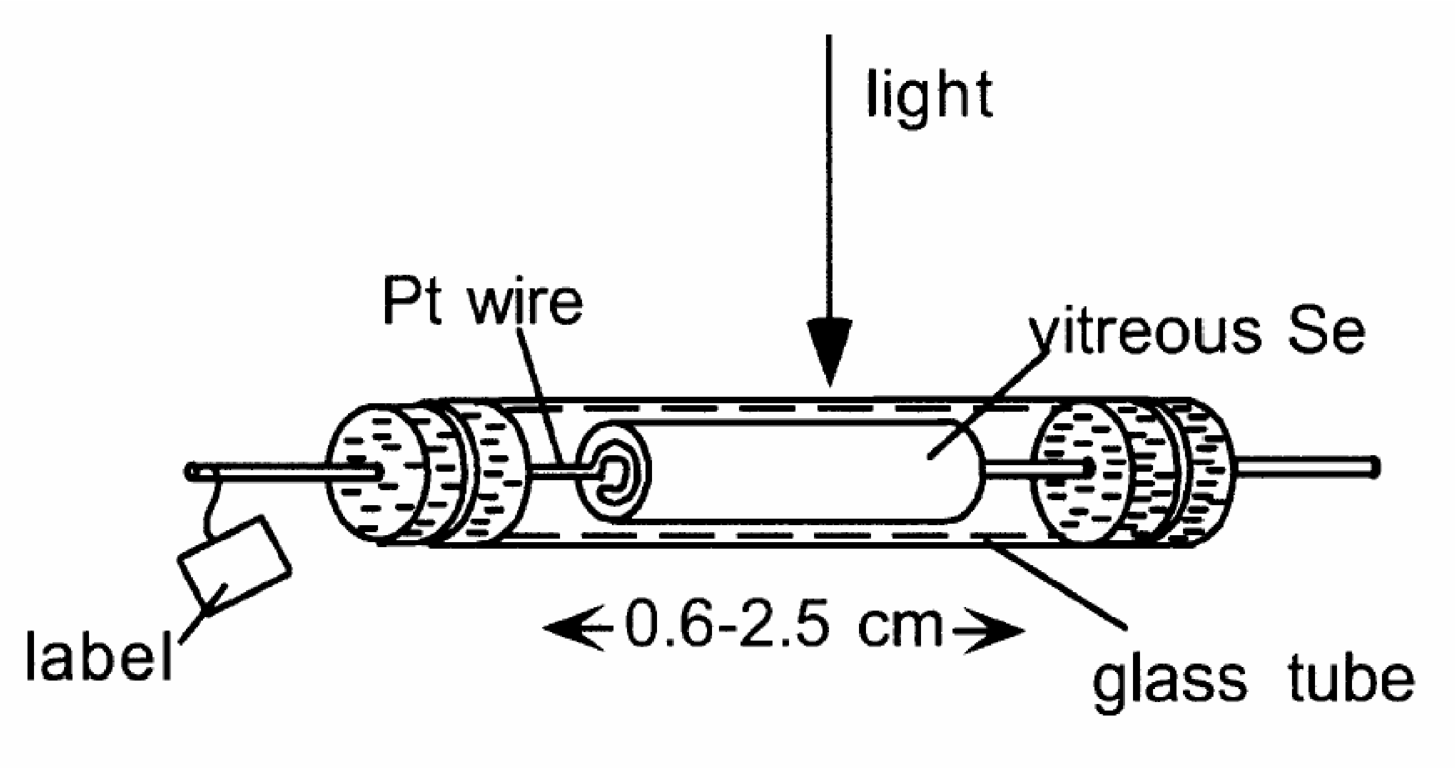

Structure of the most efficient photovoltaic devices developed during the 1930s

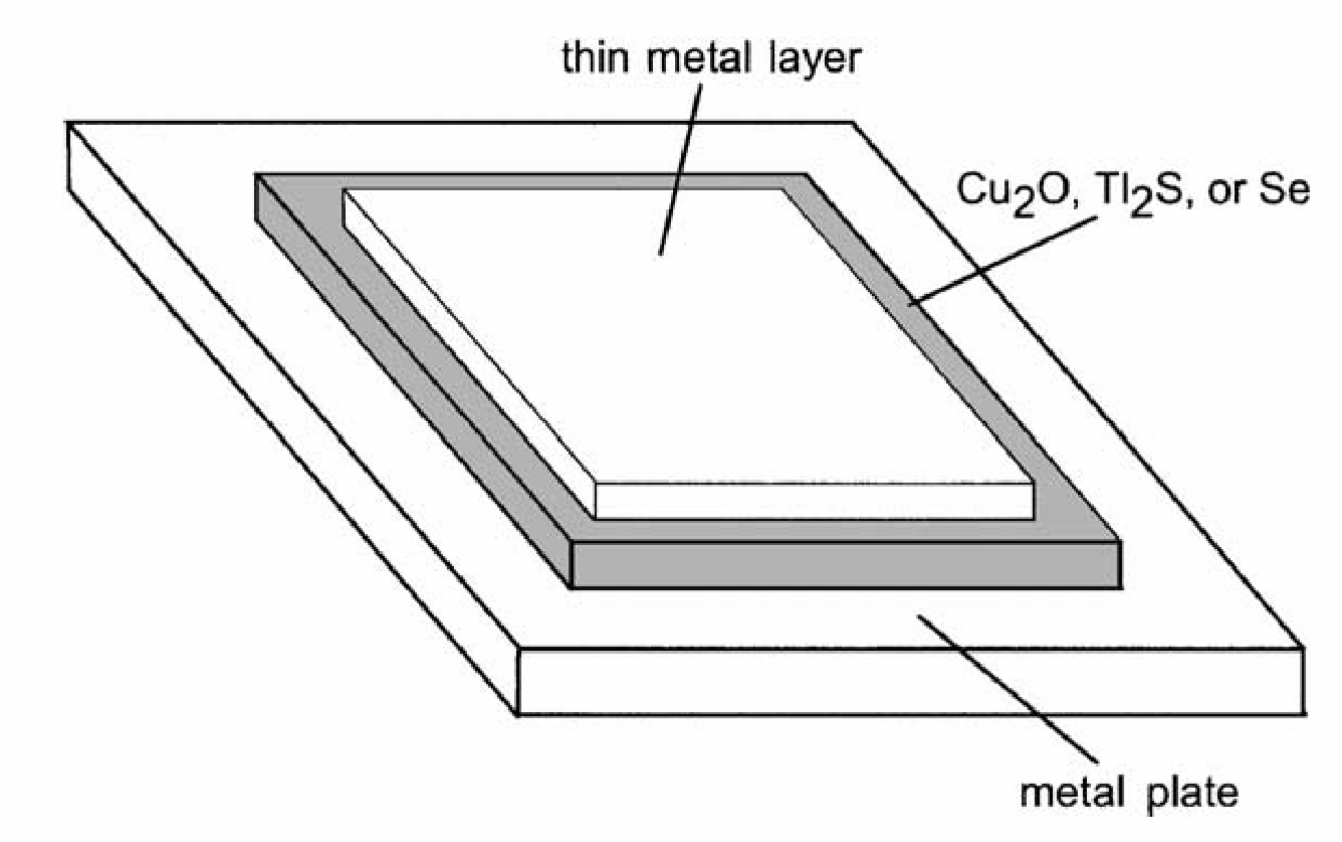

Silicon solar cell reported in 1941 (R.S. Ohl) relying on ‘grown-in’ junctions formed by impurity segregation in recrystallised silicon melts

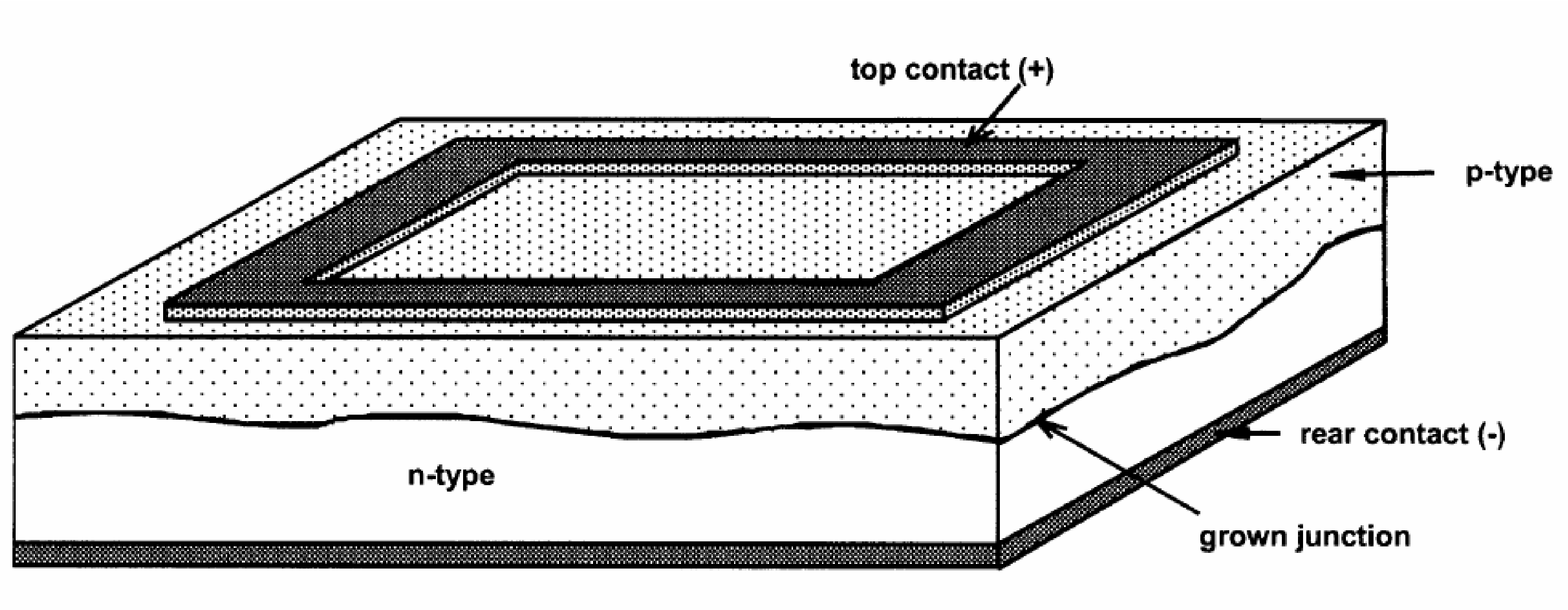

A p–n junction formed by bringing the isolated p- and n-type regions together and the corresponding energy-band diagram at thermal equilibrium

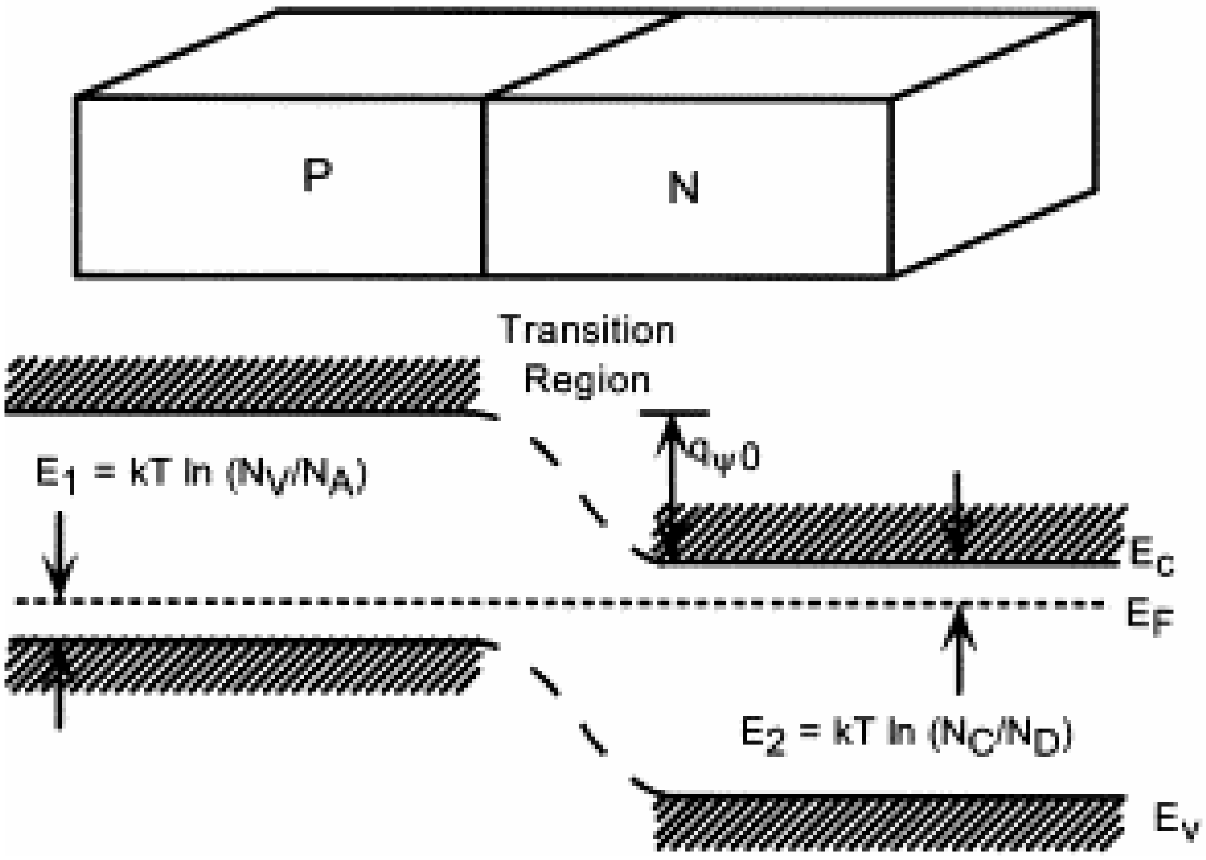

Schematic construction of a p-n homodiode

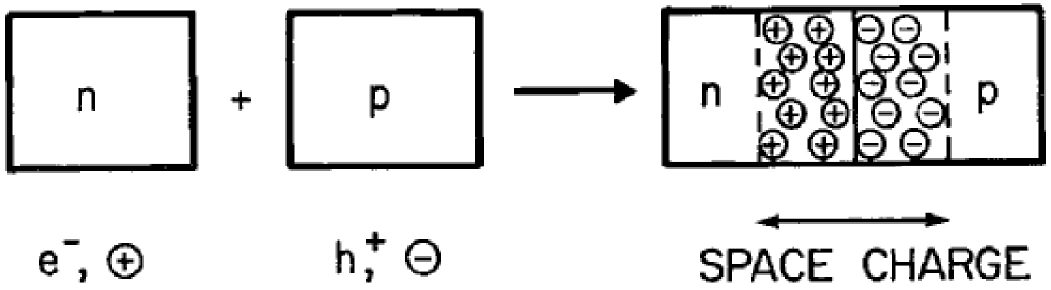

(b)

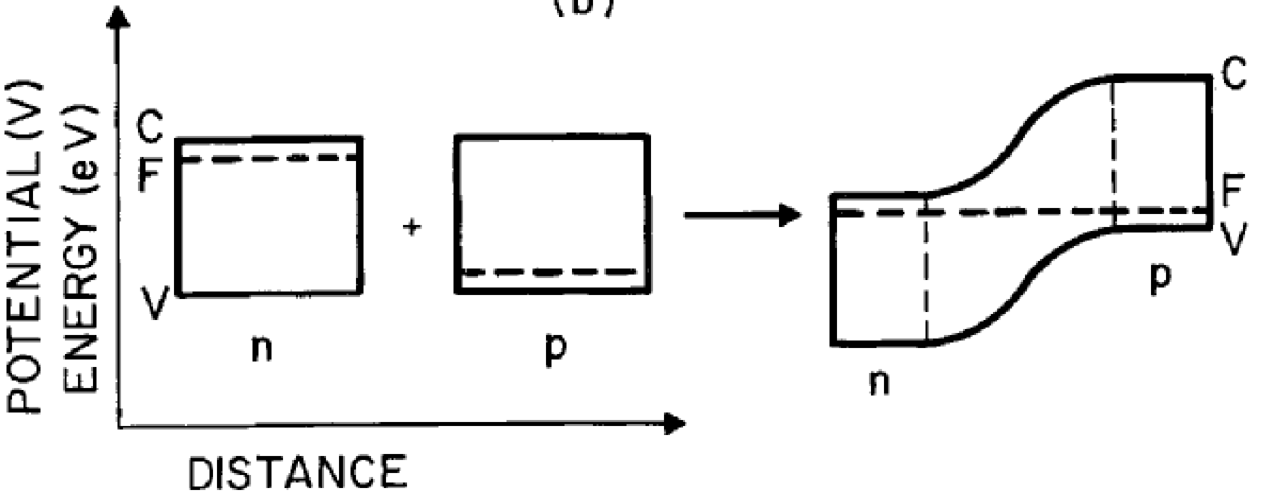

Band diagram of a homodiode solar cell

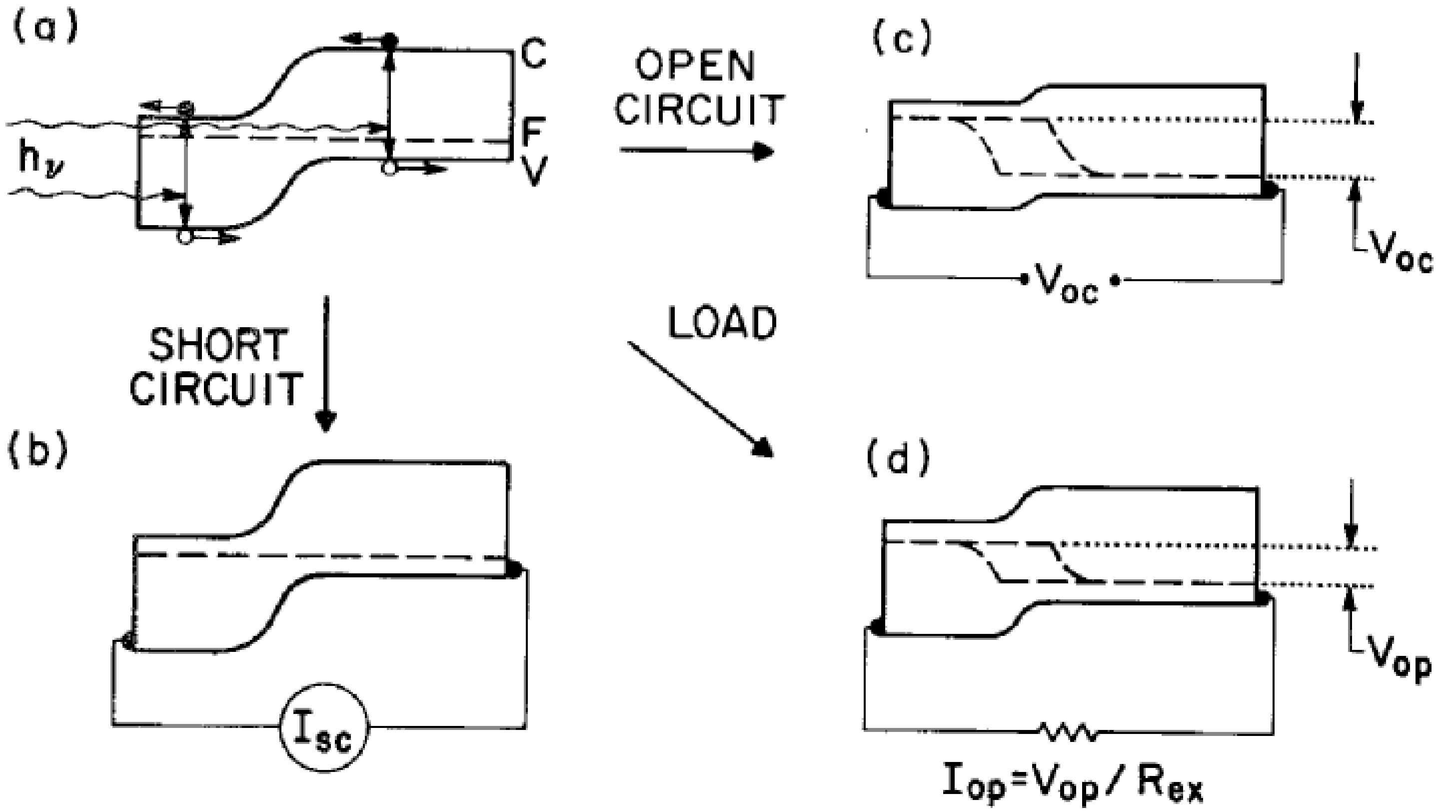

(a) creation of electron-hole pairs by absorption of light quanta
(b) short circuit condition
(c) open circuit condition
(d) under finite external load

Band diagrams of a homodiode, a heterodiode, and a Schottky barrier diode

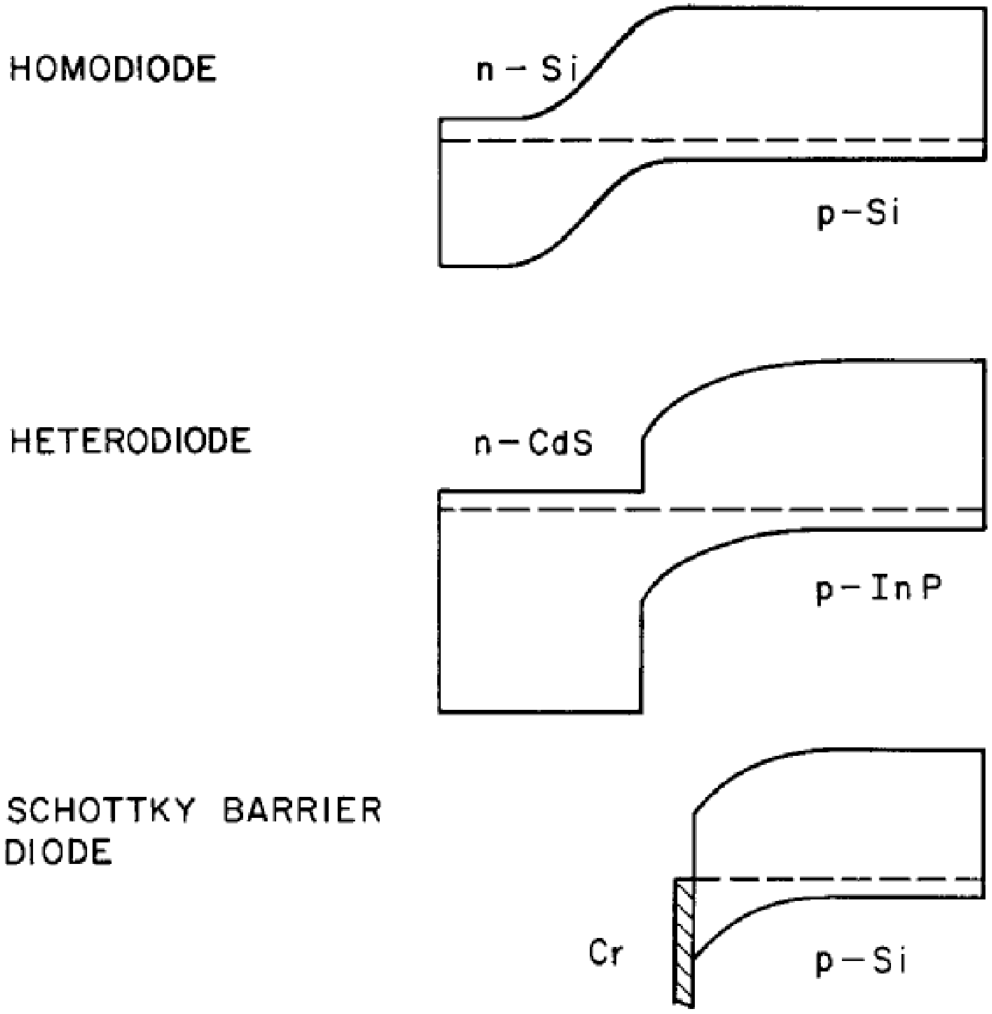

Efficiency loss processes in a p–n junction solar cell

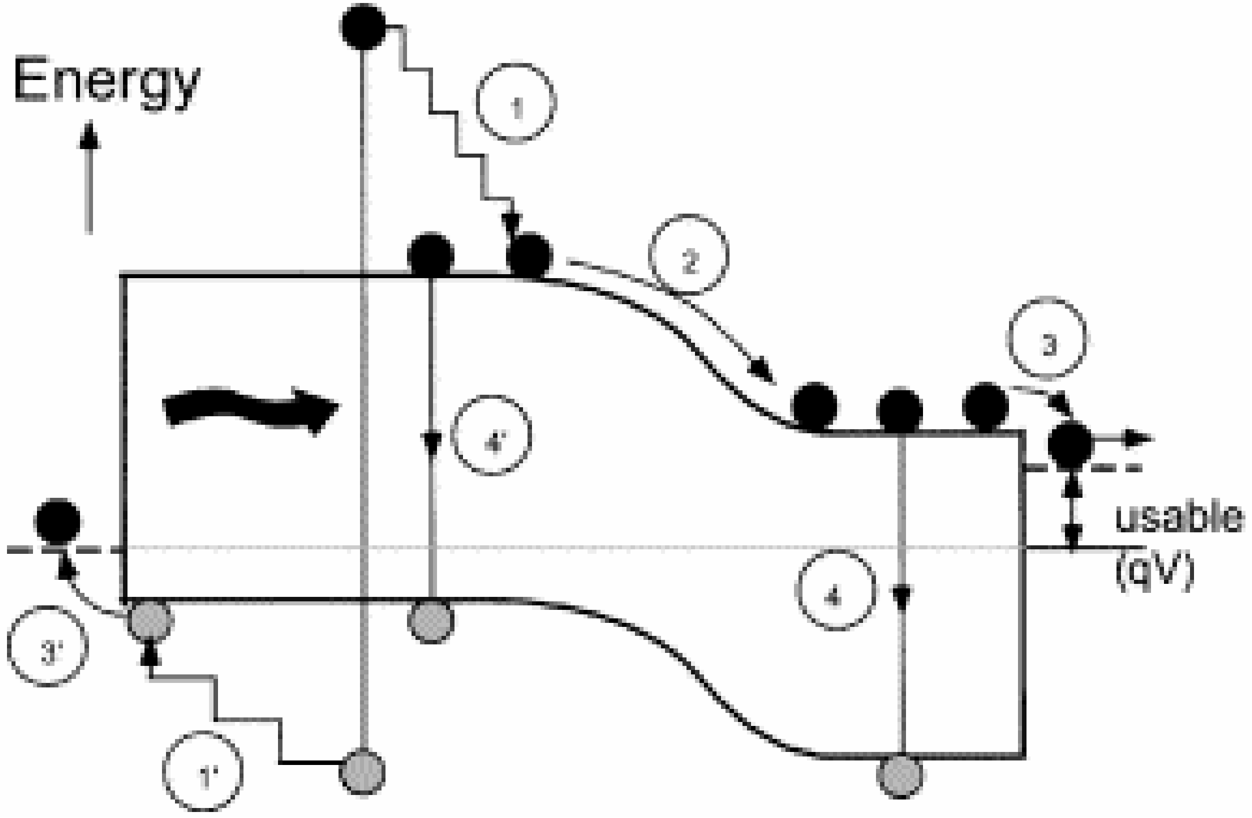

(1) thermalisation loss;
(2) junction loss;
(3) contact loss;
(4) recombination loss.

Absorption of a photon in direct gap semiconductor and indirect gap semiconductor with phonon assistance

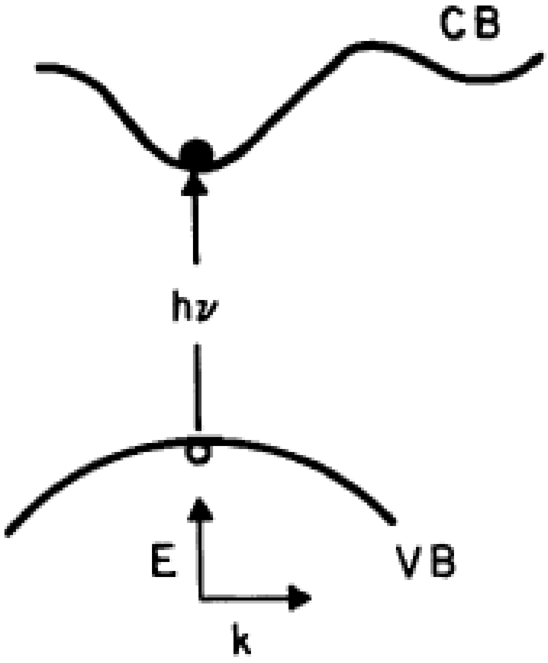

Direct gap

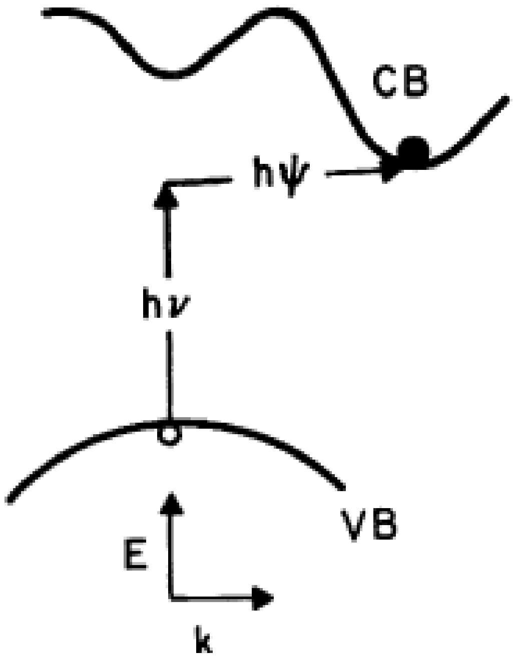

Indirect gap

Absorption coefficient (α) and absorption length ($1/\alpha$) for a typical direct-gap semiconductor, InP, and a typical indirect gap semiconductor, Si

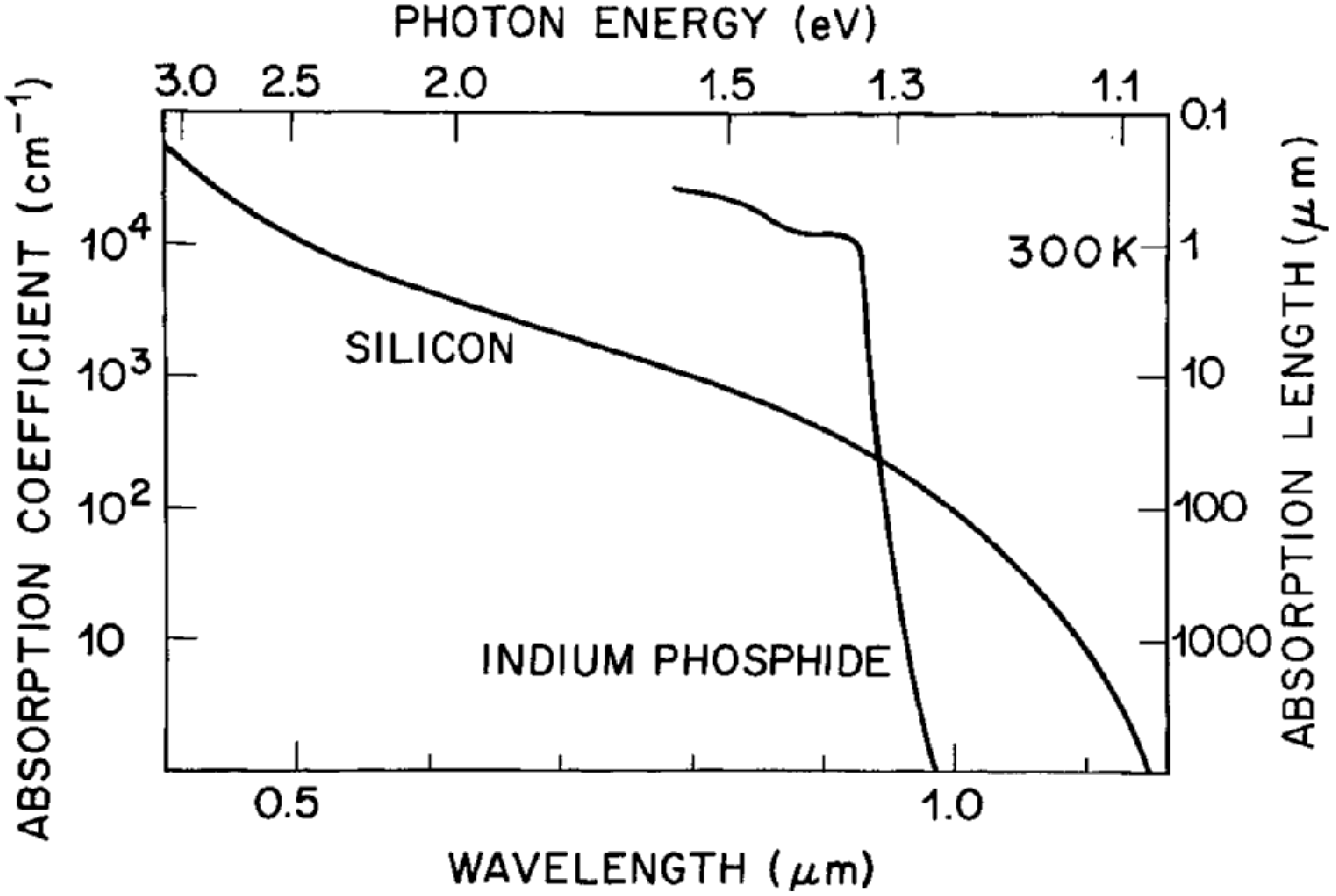

Properties of semiconductors used in solar cells

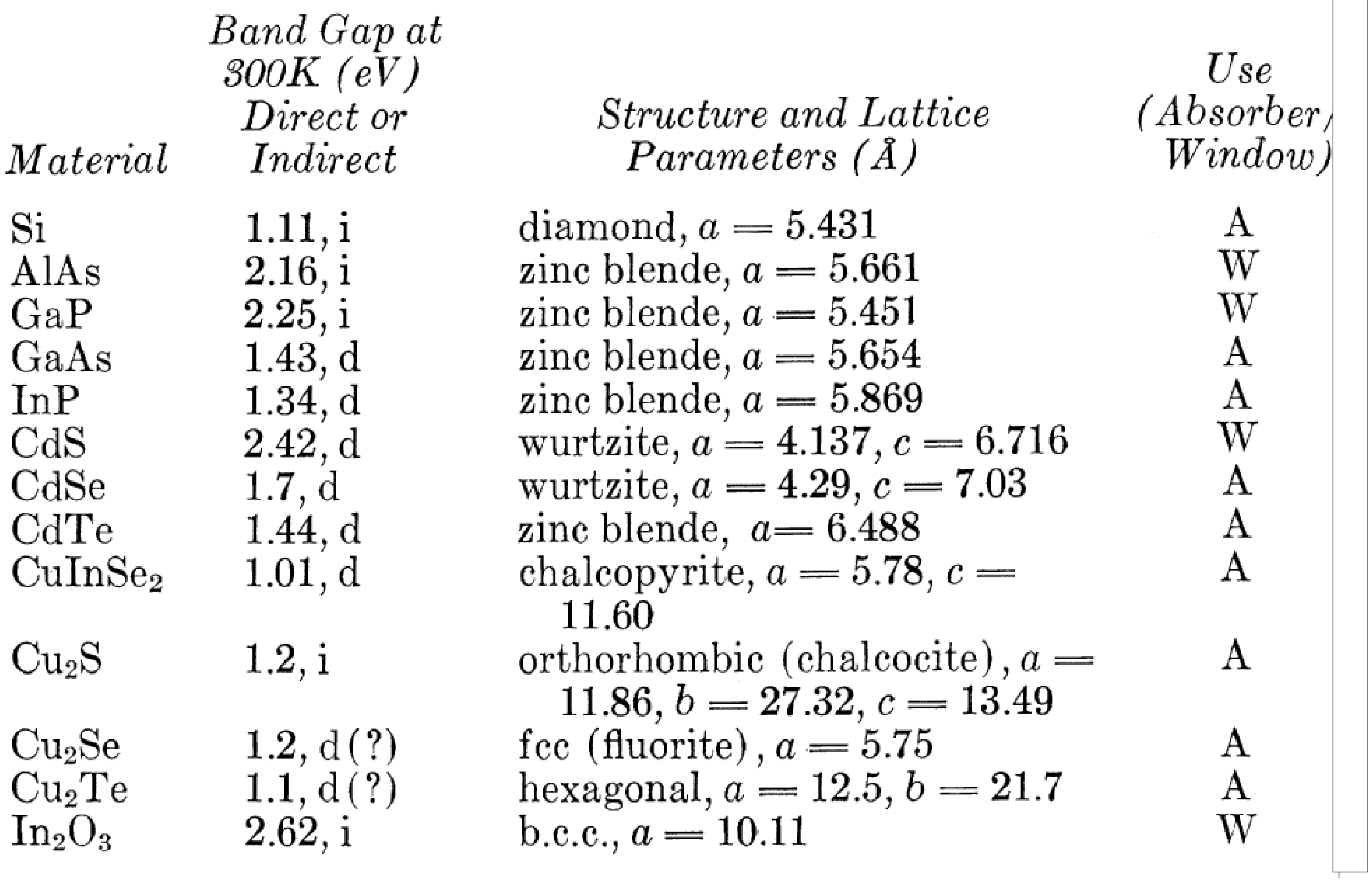

Material	*Band Gap at 300K (eV) Direct or Indirect*	*Structure and Lattice Parameters (Å)*	*Use (Absorber/ Window)*
Si	1.11, i	diamond, $a = 5.431$	A
AlAs	2.16, i	zinc blende, $a = 5.661$	W
GaP	2.25, i	zinc blende, $a = 5.451$	W
GaAs	1.43, d	zinc blende, $a = 5.654$	A
InP	1.34, d	zinc blende, $a = 5.869$	A
CdS	2.42, d	wurtzite, $a = 4.137$, $c = 6.716$	W
CdSe	1.7, d	wurtzite, $a = 4.29$, $c = 7.03$	A
CdTe	1.44, d	zinc blende, $a = 6.488$	A
$CuInSe_2$	1.01, d	chalcopyrite, $a = 5.78$, $c = 11.60$	A
Cu_2S	1.2, i	orthorhombic (chalcocite), $a = 11.86$, $b = 27.32$, $c = 13.49$	A
Cu_2Se	1.2, d(?)	fcc (fluorite), $a = 5.75$	A
Cu_2Te	1.1, d(?)	hexagonal, $a = 12.5$, $b = 21.7$	A
In_2O_3	2.62, i	b.c.c., $a = 10.11$	W

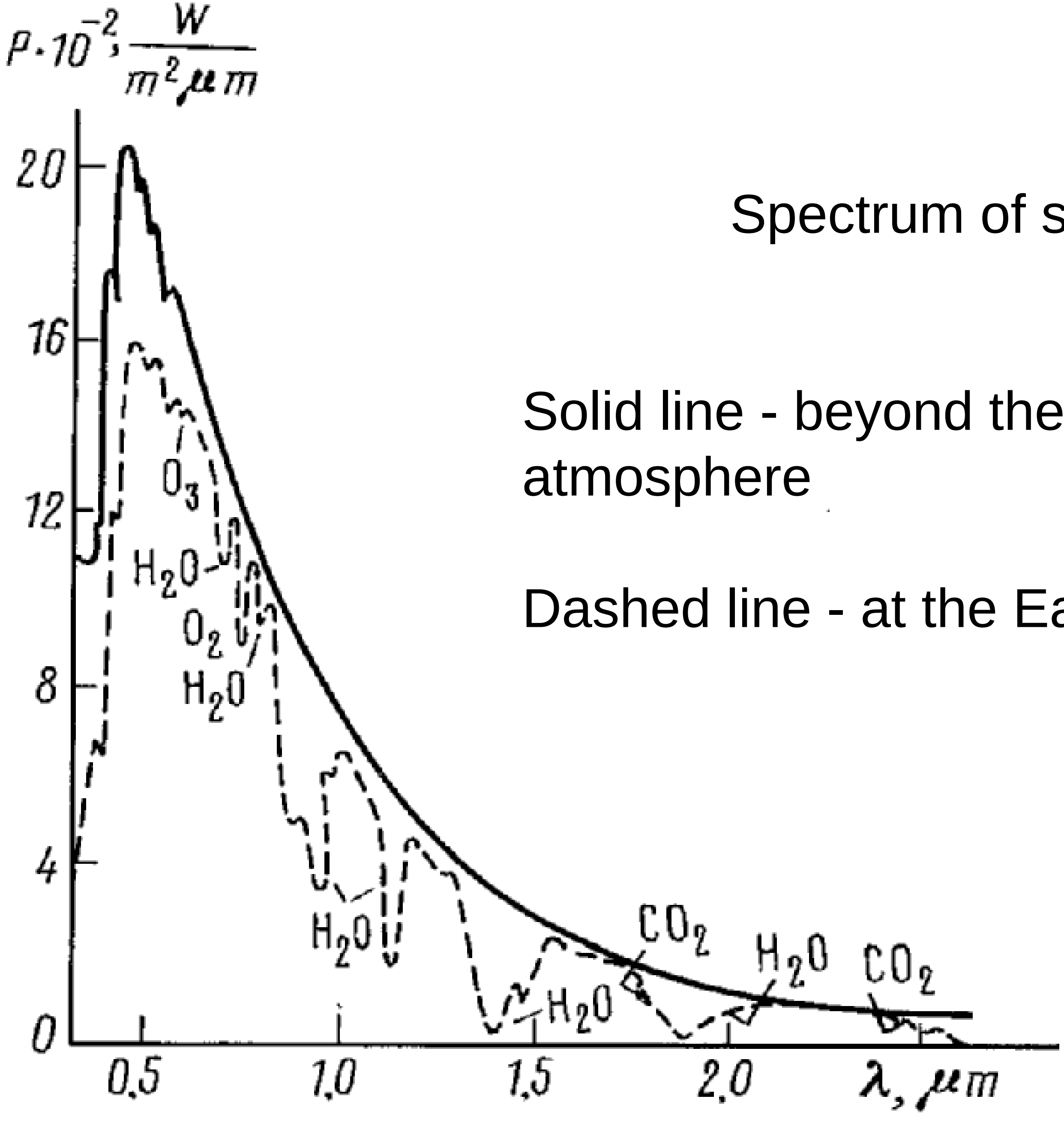

Spectrum of sunlight

Solid line - beyond the terrestrial atmosphere

Dashed line - at the Earth's surface

Crystalline silicon

First generation cells consist of high quality and single junction devices. First generation technologies involve high energy and labor inputs which prevent any significant progress in reducing production costs. Single junction silicon devices are approaching the theoretical limiting efficiency (Shockley and Queisser) of 31% and achieve cost parity with fossil fuel energy generation after a payback period of 5–7 years.

The bulk technologies are often referred to as wafer-based manufacturing - self-supporting wafers between 180 to 240 micrometers thick are processed and then soldered together to form a solar cell module.

The most prevalent bulk material for solar cells is crystalline silicon (abbreviated as c-Si), also known as "solar grade silicon". Bulk silicon is separated into multiple categories according to crystallinity and crystal size in the resulting ingot, ribbon, or wafer.

Monocrystalline silicon (c-Si): often made using the Czochralski process. Single-crystal wafer cells tend to be expensive, and because they are cut from cylindrical ingots, do not completely cover a square solar cell module without a substantial waste of refined silicon.

Ribbon silicon is a type of monocrystalline silicon: it is formed by drawing flat thin films from molten silicon and having a multicrystalline structure. These cells have lower efficiencies than poly-Si, but save on production costs due to a great reduction in silicon waste, as this approach does not require sawing from ingots.

Poly- or *multicrystalline silicon* (poly-Si or mc-Si): made from cast square ingots — large blocks of molten silicon carefully cooled and solidified. Poly-Si cells are less expensive to produce than single crystal silicon cells, but are less efficient.

Standard silicon solar cell structure developed in the 1970s

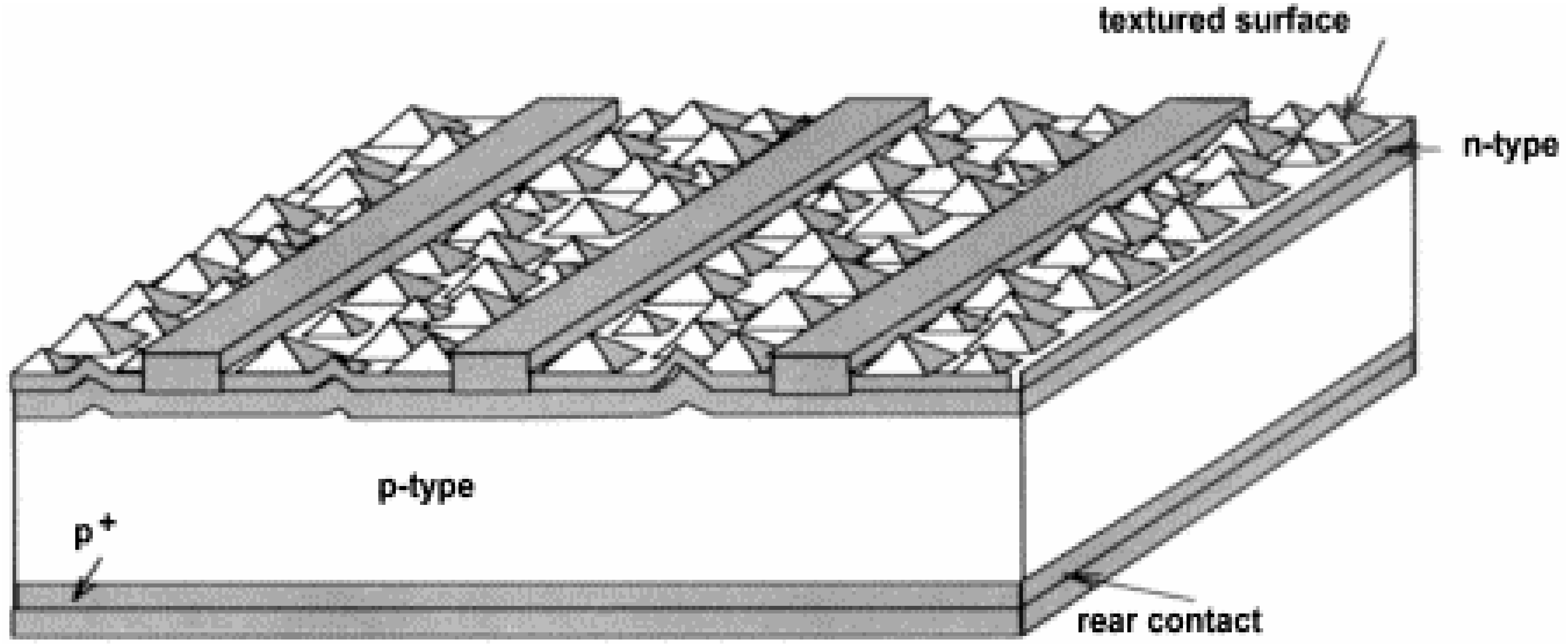

Thin-film cells

Second generation materials have been developed to address energy requirements and production costs of solar cells. Alternative manufacturing techniques such as vapour deposition, electroplating, and use of ultrasonic nozzles are advantageous as they reduce high temperature processing significantly.

Silicon thin-film cells are mainly deposited by chemical vapor deposition (typically plasma-enhanced (PE-CVD)) from silane gas and hydrogen gas. Depending on the deposition parameters, this can yield:

1. Amorphous silicon (a-Si or a-Si:H)
2. Protocrystalline silicon or
3. Nanocrystalline silicon (nc-Si or nc-Si:H), also called microcrystalline silicon.

These types of silicon present dangling and twisted bonds, which results in deep defects (energy levels in the bandgap) as well as deformation of the valence and conduction bands (band tails). The solar cells made from these materials tend to have lower energy conversion efficiency than bulk silicon, but are also less expensive to produce.

Amorphous silicon has a higher bandgap (1.7 eV) than crystalline silicon (c-Si) (1.1 eV), which means it absorbs the visible part of the solar spectrum more strongly than the infrared portion of the spectrum. As nc-Si has about the same bandgap as c-Si, the nc-Si and a-Si can advantageously be combined in thin layers, creating a layered cell called a tandem cell. The top cell in a-Si absorbs the visible light and leaves the infrared part of the spectrum for the bottom cell in nanocrystalline Si.

Recently, solutions to overcome the limitations of thin-film crystalline silicon have been developed. Light trapping schemes where the weakly absorbed long wavelength light is obliquely coupled into the silicon and traverses the film several times can significantly enhance the absorption of sunlight in the thin silicon films. Thermal processing techniques can significantly enhance the crystal quality of the silicon and thereby lead to higher efficiencies of the final solar cells.

Microcrystalline and amorphous silicon tandem solar cell, so-called "micromorph" solar cell

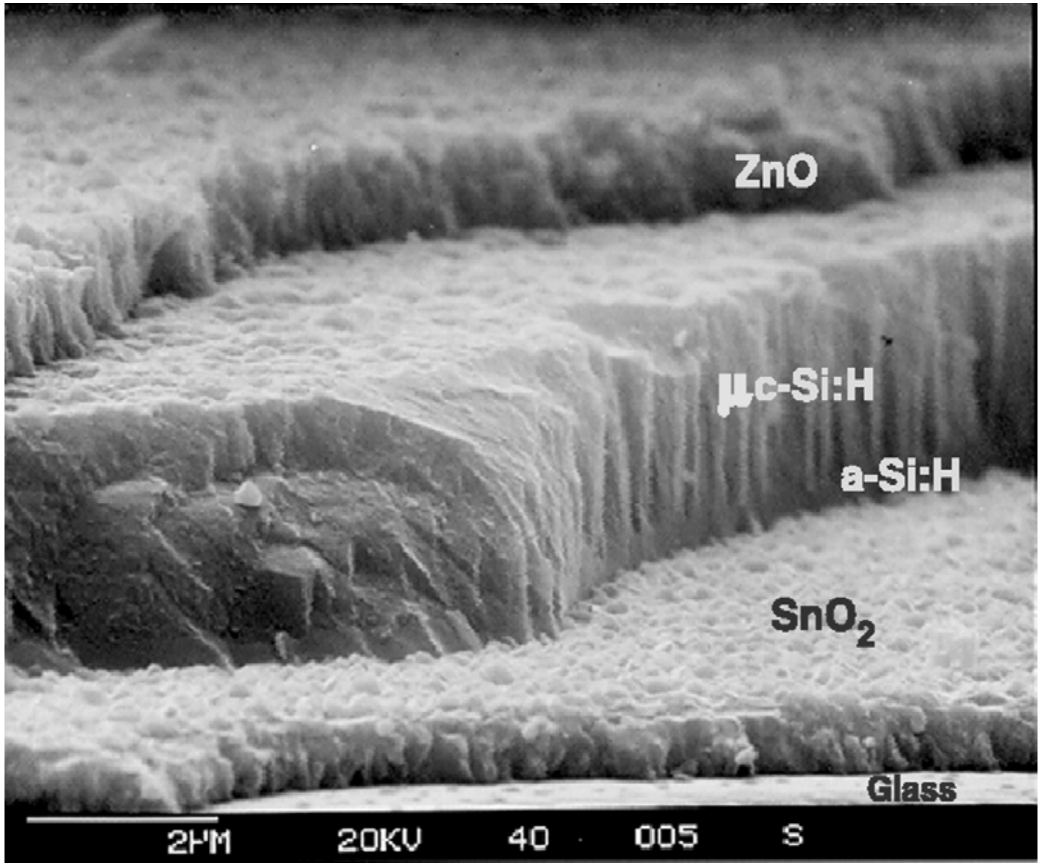

A cadmium telluride solar cell is based on an efficient light-absorbing material for thin-film cells. Compared to other thin-film materials, CdTe is easier to deposit and more suitable for large-scale production.

The materials based on $CuInSe_2$ that are of interest for photovoltaic applications include several elements from groups I, III and VI in the periodic table. These semiconductors are especially attractive for thin film solar cell application because of their high optical absorption coefficients and versatile optical and electrical characteristics which can in principle be manipulated and tuned for a specific need in a given device. When gallium is substituted for some of the indium in CIS, the material is referred to as CIGS, or copper indium/gallium diselenide, a solid mixture of the semiconductors $CuInSe_2$ and $CuGaSe_2$, abbreviated by the chemical formula $CuIn_xGa_{(1-x)}Se_2$.

Photocurrent-photovoltage curve of a p$CuInSe_2$/nCdS heterodiode under 92 mW cm^{-2} solar illumination

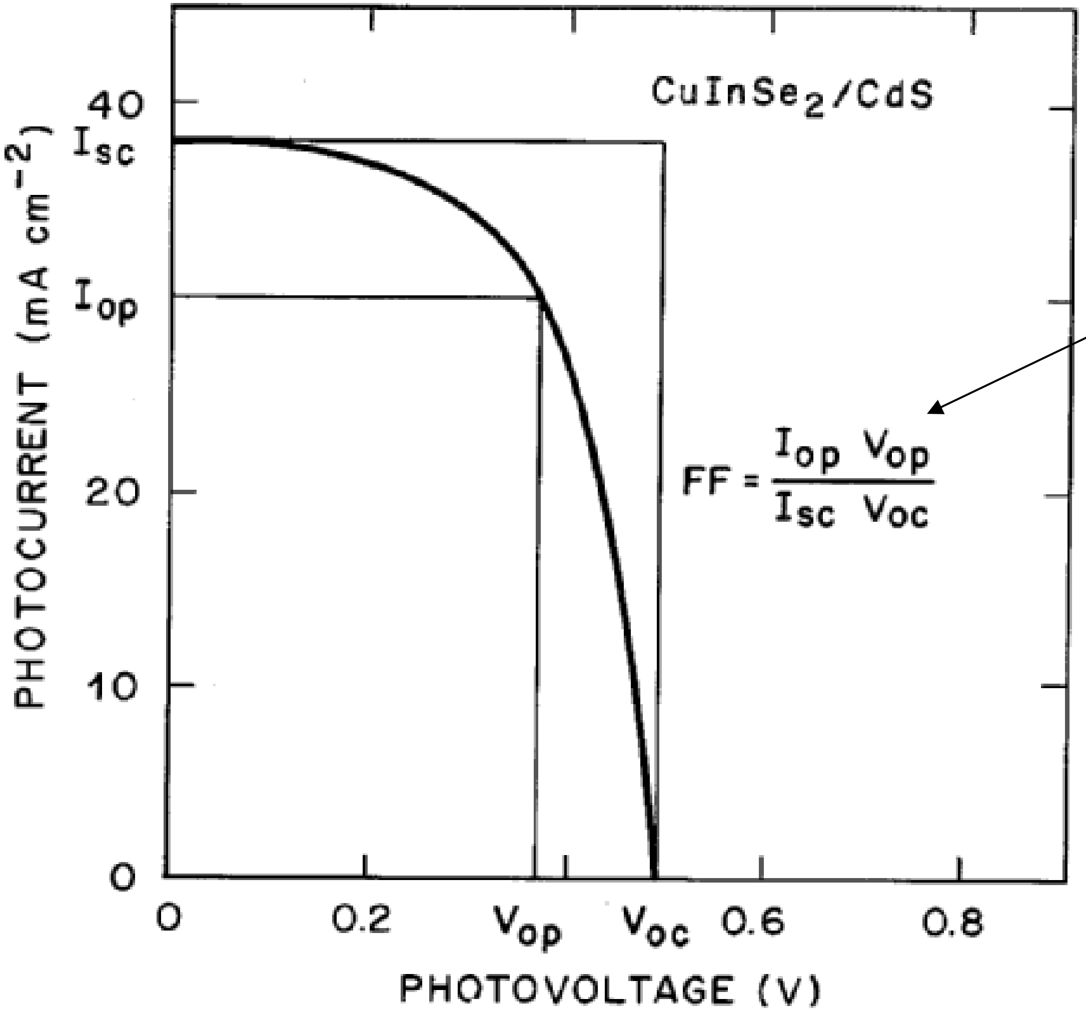

Definition of the fill factor FF

In 2007 First Solar produced 200 MW of CdTe solar cells.Wurth Solar commercialised its CIS technology in 2007 producing 15 MW. Nanosolar commercialised its CIGS technology in 2007 with a production capacity of 430 MW for 2008 in the USA and Germany.

In 2007, CdTe production represented 4.7% of total market share, thin-film silicon 5.2% and CIGS 0.5%.

Gallium arsenide (GaAs) multijunction

High-efficiency multijunction cells were originally developed for special applications such as satellites and space exploration (Mars rover missions), but at present, their use in terrestrial concentrators might be the lowest cost alternative in terms of \$/kWh and \$/W. These multijunction cells consist of multiple thin films produced using metalorganic vapour phase epitaxy. A triple-junction cell, for example, may consist of the semiconductors: GaAs, Ge, and $GaInP_2$. Each type of semiconductor will have a characteristic band gap energy which, loosely speaking, causes it to absorb light most efficiently at a certain color, or more precisely, to absorb electromagnetic radiation over a portion of the spectrum. The semiconductors are carefully chosen to absorb nearly all of the solar spectrum.

Schematic of full tandem structure

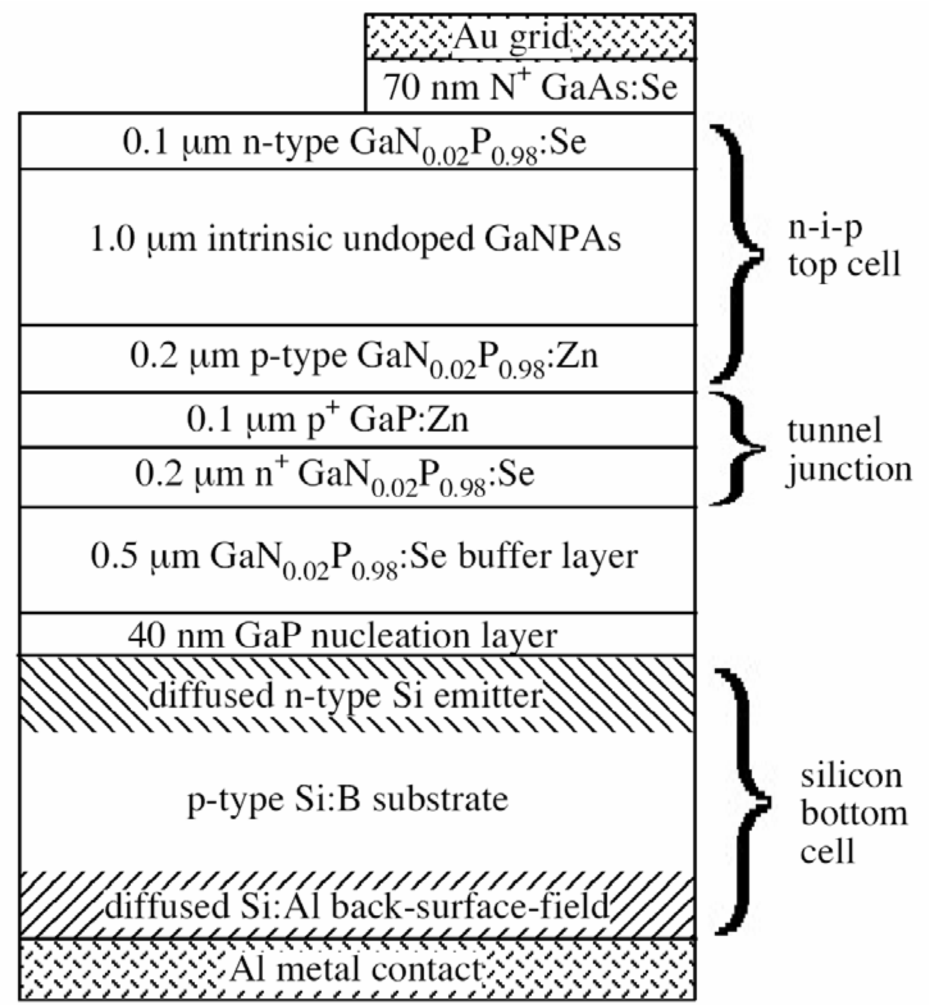

GaAs based multijunction devices are the most efficient solar cells to date, reaching a record high of 40.7% efficiency under solar concentration and laboratory conditions.Tandem solar cells based on monolithic, series connected, gallium indium phosphide (GaInP), gallium arsenide GaAs, and germanium Ge pn junctions.

Thin film solar cells: In 2002, the highest reported efficiency for solar cells based on thin films of CdTe is 18% (Sheffield Hallam University).

The US national renewable energy research facility NREL achieved an efficiency of 19.9% for the solar cells based on copper indium gallium selenide. These CIGS films have been grown by physical vapour deposition in a three-stage co-evaporation process. In this process In, Ga and Se are evaporated in the first step; in the second step it is followed by Cu and Se co-evaporation and in the last step terminated by In, Ga and Se evaporation again.

Confirmed terrestrial cell and submodule efficiencies measured under the global AM1.5 spectrum (1000 Wm^2)

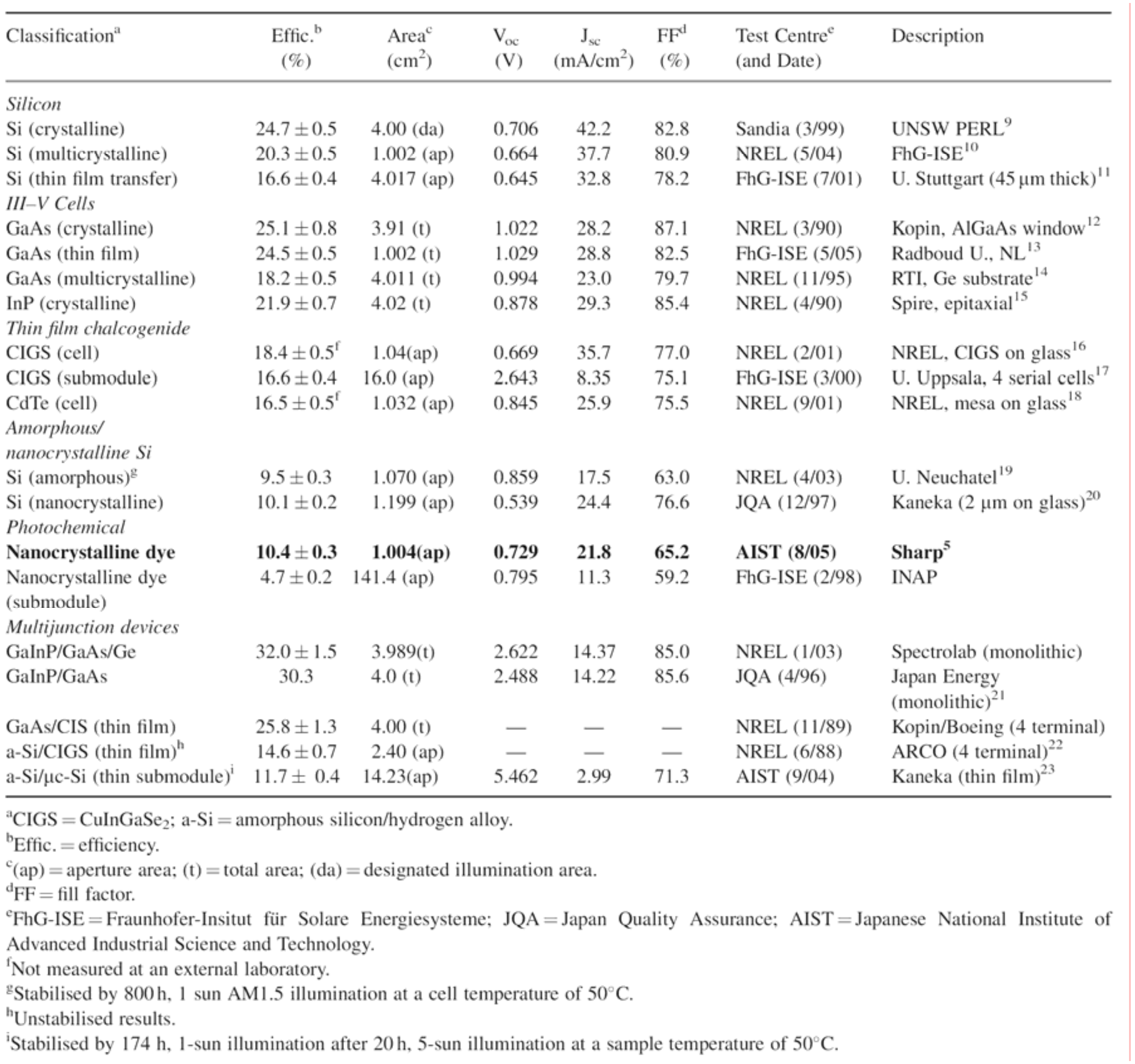

Classification[a]	Effic.[b] (%)	Area[c] (cm^2)	V_{oc} (V)	J_{sc} (mA/cm^2)	FF[d] (%)	Test Centre[e] (and Date)	Description
Silicon							
Si (crystalline)	24.7 ± 0.5	4.00 (da)	0.706	42.2	82.8	Sandia (3/99)	UNSW PERL[9]
Si (multicrystalline)	20.3 ± 0.5	1.002 (ap)	0.664	37.7	80.9	NREL (5/04)	FhG-ISE[10]
Si (thin film transfer)	16.6 ± 0.4	4.017 (ap)	0.645	32.8	78.2	FhG-ISE (7/01)	U. Stuttgart (45 μm thick)[11]
III–V Cells							
GaAs (crystalline)	25.1 ± 0.8	3.91 (t)	1.022	28.2	87.1	NREL (3/90)	Kopin, AlGaAs window[12]
GaAs (thin film)	24.5 ± 0.5	1.002 (t)	1.029	28.8	82.5	FhG-ISE (5/05)	Radboud U., NL[13]
GaAs (multicrystalline)	18.2 ± 0.5	4.011 (t)	0.994	23.0	79.7	NREL (11/95)	RTI, Ge substrate[14]
InP (crystalline)	21.9 ± 0.7	4.02 (t)	0.878	29.3	85.4	NREL (4/90)	Spire, epitaxial[15]
Thin film chalcogenide							
CIGS (cell)	18.4 ± 0.5[f]	1.04(ap)	0.669	35.7	77.0	NREL (2/01)	NREL, CIGS on glass[16]
CIGS (submodule)	16.6 ± 0.4	16.0 (ap)	2.643	8.35	75.1	FhG-ISE (3/00)	U. Uppsala, 4 serial cells[17]
CdTe (cell)	16.5 ± 0.5[f]	1.032 (ap)	0.845	25.9	75.5	NREL (9/01)	NREL, mesa on glass[18]
Amorphous/ nanocrystalline Si							
Si (amorphous)[g]	9.5 ± 0.3	1.070 (ap)	0.859	17.5	63.0	NREL (4/03)	U. Neuchatel[19]
Si (nanocrystalline)	10.1 ± 0.2	1.199 (ap)	0.539	24.4	76.6	JQA (12/97)	Kaneka (2 μm on glass)[20]
Photochemical							
Nanocrystalline dye	**10.4 ± 0.3**	**1.004(ap)**	**0.729**	**21.8**	**65.2**	**AIST (8/05)**	**Sharp**[5]
Nanocrystalline dye (submodule)	4.7 ± 0.2	141.4 (ap)	0.795	11.3	59.2	FhG-ISE (2/98)	INAP
Multijunction devices							
GaInP/GaAs/Ge	32.0 ± 1.5	3.989(t)	2.622	14.37	85.0	NREL (1/03)	Spectrolab (monolithic)
GaInP/GaAs	30.3	4.0 (t)	2.488	14.22	85.6	JQA (4/96)	Japan Energy (monolithic)[21]
GaAs/CIS (thin film)	25.8 ± 1.3	4.00 (t)	—	—	—	NREL (11/89)	Kopin/Boeing (4 terminal)
a-Si/CIGS (thin film)[h]	14.6 ± 0.7	2.40 (ap)	—	—	—	NREL (6/88)	ARCO (4 terminal)[22]
a-Si/μc-Si (thin submodule)[i]	11.7 ± 0.4	14.23(ap)	5.462	2.99	71.3	AIST (9/04)	Kaneka (thin film)[23]

[a] CIGS = $CuInGaSe_2$; a-Si = amorphous silicon/hydrogen alloy.

[b] Effic. = efficiency.

[c] (ap) = aperture area; (t) = total area; (da) = designated illumination area.

[d] FF = fill factor.

[e] FhG-ISE = Fraunhofer-Insitut für Solare Energiesysteme; JQA = Japan Quality Assurance; AIST = Japanese National Institute of Advanced Industrial Science and Technology.

[f] Not measured at an external laboratory.

[g] Stabilised by 800 h, 1 sun AM1.5 illumination at a cell temperature of 50°C.

[h] Unstabilised results.

[i] Stabilised by 174 h, 1-sun illumination after 20 h, 5-sun illumination at a sample temperature of 50°C.

Confirmed terrestrial module efficiencies measured under the global AM1.5 spectrum (1000W/m2) at a cell temperature of 25°C

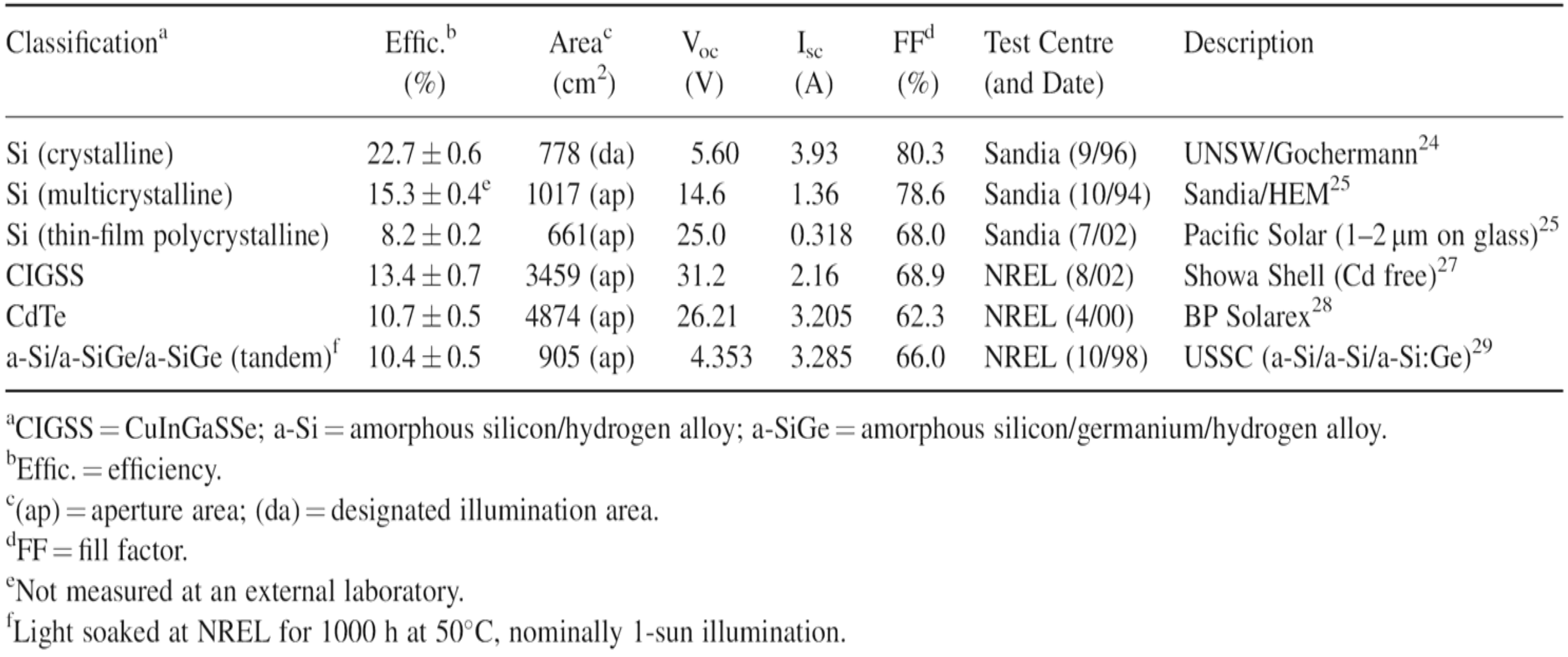

Classification[a]	Effic.[b] (%)	Area[c] (cm^2)	V_{oc} (V)	I_{sc} (A)	FF[d] (%)	Test Centre (and Date)	Description
Si (crystalline)	22.7 ± 0.6	778 (da)	5.60	3.93	80.3	Sandia (9/96)	UNSW/Gochermann[24]
Si (multicrystalline)	15.3 ± 0.4[e]	1017 (ap)	14.6	1.36	78.6	Sandia (10/94)	Sandia/HEM[25]
Si (thin-film polycrystalline)	8.2 ± 0.2	661(ap)	25.0	0.318	68.0	Sandia (7/02)	Pacific Solar (1–2 μm on glass)[25]
CIGSS	13.4 ± 0.7	3459 (ap)	31.2	2.16	68.9	NREL (8/02)	Showa Shell (Cd free)[27]
CdTe	10.7 ± 0.5	4874 (ap)	26.21	3.205	62.3	NREL (4/00)	BP Solarex[28]
a-Si/a-SiGe/a-SiGe (tandem)[f]	10.4 ± 0.5	905 (ap)	4.353	3.285	66.0	NREL (10/98)	USSC (a-Si/a-Si/a-Si:Ge)[29]

[a] CIGSS = CuInGaSSe; a-Si = amorphous silicon/hydrogen alloy; a-SiGe = amorphous silicon/germanium/hydrogen alloy.

[b] Effic. = efficiency.

[c] (ap) = aperture area; (da) = designated illumination area.

[d] FF = fill factor.

[e] Not measured at an external laboratory.

[f] Light soaked at NREL for 1000 h at 50°C, nominally 1-sun illumination.

“Top ten” confirmed cell and module results, not class records (Global AM1.5 spectrum,1000 Wm^{-2}, 25°C)

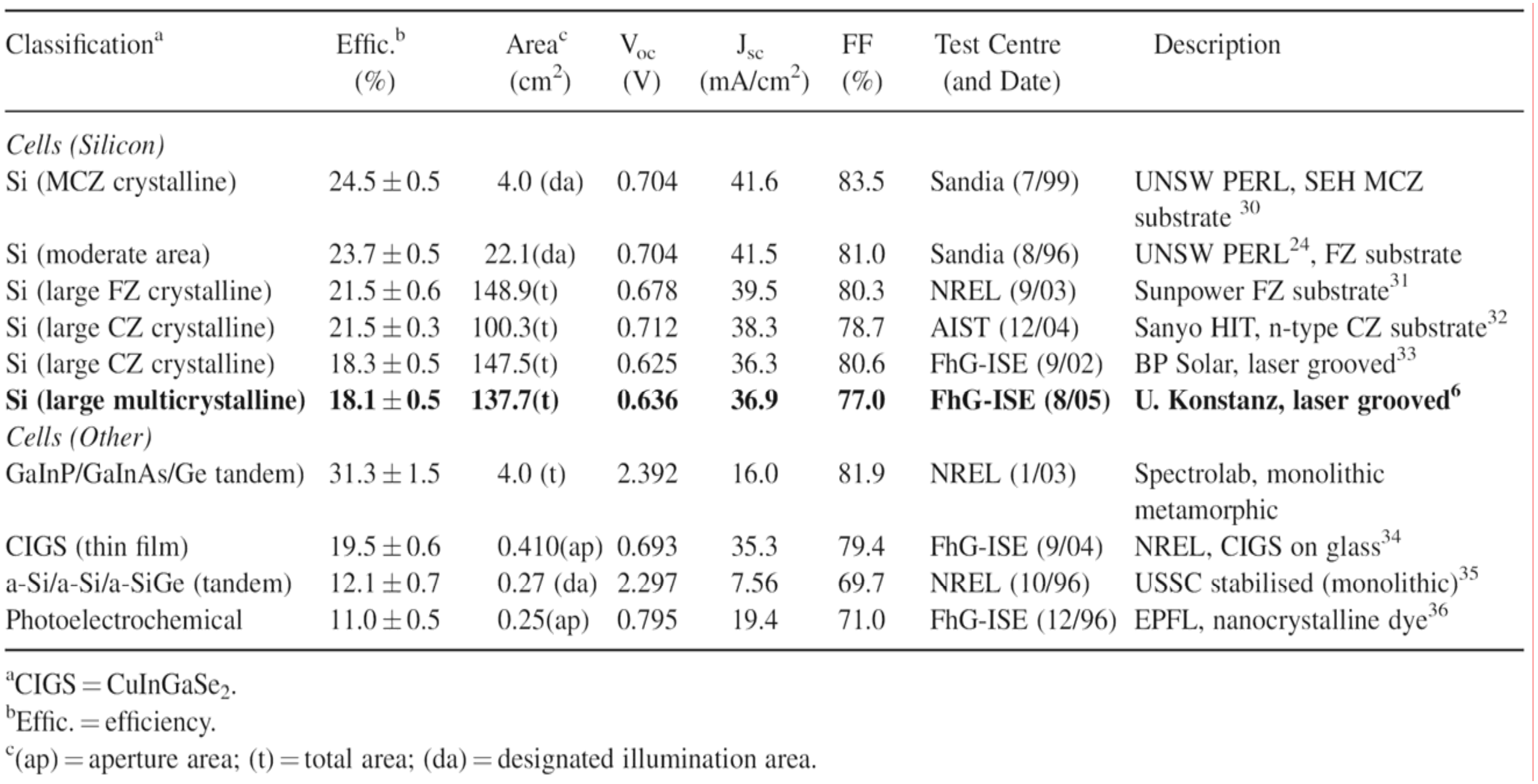

Classification[a]	Effic.[b] (%)	Area[c] (cm^2)	V_{oc} (V)	J_{sc} (mA/cm^2)	FF (%)	Test Centre (and Date)	Description
Cells (Silicon)							
Si (MCZ crystalline)	24.5 ± 0.5	4.0 (da)	0.704	41.6	83.5	Sandia (7/99)	UNSW PERL, SEH MCZ substrate [30]
Si (moderate area)	23.7 ± 0.5	22.1(da)	0.704	41.5	81.0	Sandia (8/96)	UNSW PERL[24], FZ substrate
Si (large FZ crystalline)	21.5 ± 0.6	148.9(t)	0.678	39.5	80.3	NREL (9/03)	Sunpower FZ substrate[31]
Si (large CZ crystalline)	21.5 ± 0.3	100.3(t)	0.712	38.3	78.7	AIST (12/04)	Sanyo HIT, n-type CZ substrate[32]
Si (large CZ crystalline)	18.3 ± 0.5	147.5(t)	0.625	36.3	80.6	FhG-ISE (9/02)	BP Solar, laser grooved[33]
Si (large multicrystalline)	**18.1 ± 0.5**	**137.7(t)**	**0.636**	**36.9**	**77.0**	**FhG-ISE (8/05)**	**U. Konstanz, laser grooved[6]**
Cells (Other)							
GaInP/GaInAs/Ge tandem)	31.3 ± 1.5	4.0 (t)	2.392	16.0	81.9	NREL (1/03)	Spectrolab, monolithic metamorphic
CIGS (thin film)	19.5 ± 0.6	0.410(ap)	0.693	35.3	79.4	FhG-ISE (9/04)	NREL, CIGS on glass[34]
a-Si/a-Si/a-SiGe (tandem)	12.1 ± 0.7	0.27 (da)	2.297	7.56	69.7	NREL (10/96)	USSC stabilised (monolithic)[35]
Photoelectrochemical	11.0 ± 0.5	0.25(ap)	0.795	19.4	71.0	FhG-ISE (12/96)	EPFL, nanocrystalline dye[36]

[a] CIGS = $CuInGaSe_2$.

[b] Effic. = efficiency.

[c] (ap) = aperture area; (t) = total area; (da) = designated illumination area.

Concentrating photovoltaic systems

They use a large area of lenses or mirrors to focus sunlight on a small area of photovoltaic cells. If these systems use single or dual-axis tracking to improve performance, they may be referred to as Heliostat Concentrator Photovoltaics (HCPV). The primary attraction of CPV systems is their reduced usage of semiconducting material which is expensive and currently in short supply. Additionally, increasing the concentration ratio improves the performance of general photovoltaic materials. Despite the advantages of CPV technologies their application has been limited by the costs of focusing, tracking and cooling equipment.

Solar Systems started in 2008 a project using this technology, Solar power station in Victoria (Australia), to be completed by 2013. This plant, at 154 MW, would be ten times larger than the largest current photovoltaic plant in the world.

Terrestrial concentrator cell and module efficiencies measured under the direct beam AM1.5 spectrum at a cell temperature of 25°C

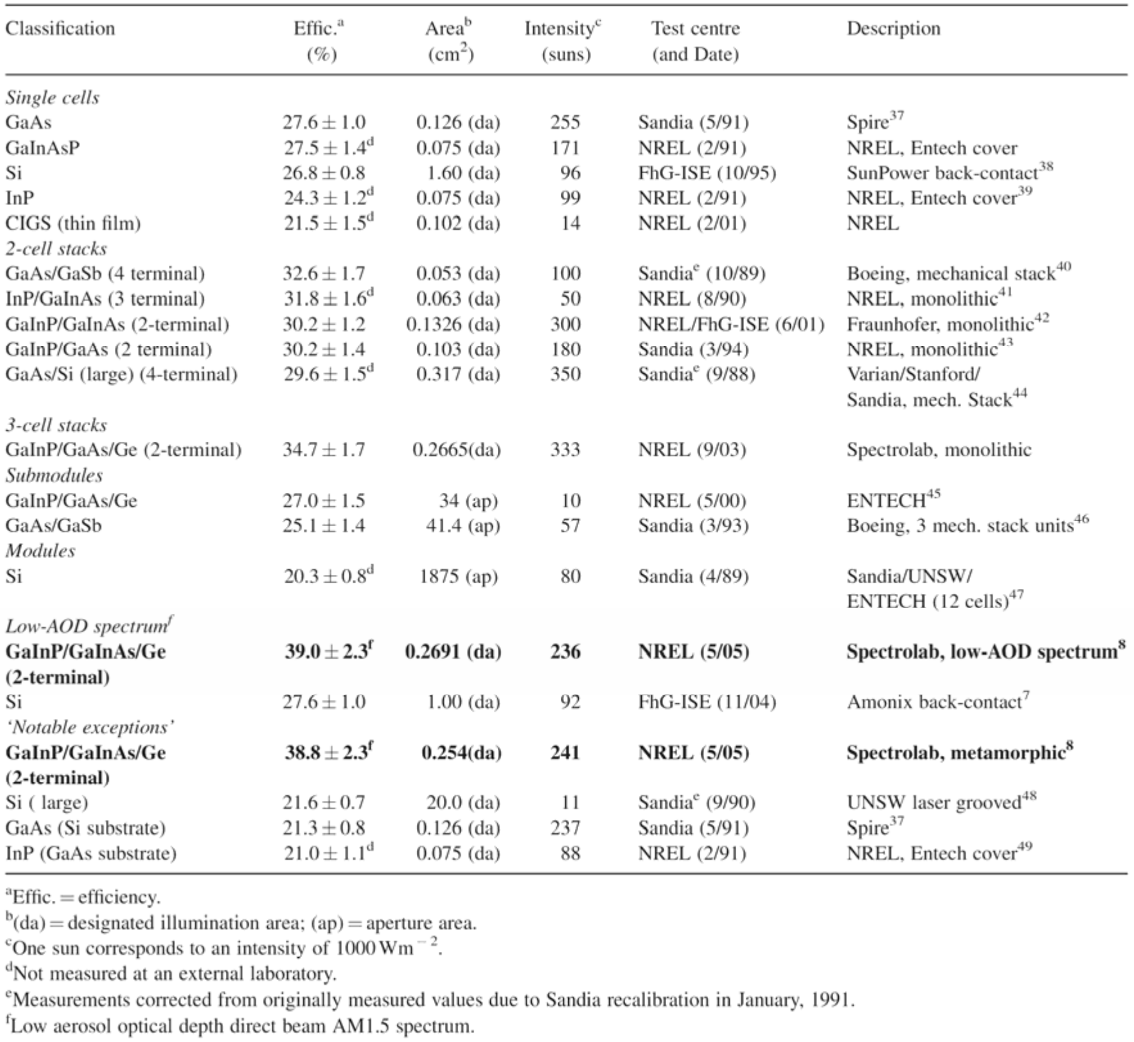

Classification	Effic.[a] (%)	Area[b] (cm^2)	Intensity[c] (suns)	Test centre (and Date)	Description
Single cells					
GaAs	27.6 ± 1.0	0.126 (da)	255	Sandia (5/91)	Spire[37]
GaInAsP	27.5 ± 1.4[d]	0.075 (da)	171	NREL (2/91)	NREL, Entech cover
Si	26.8 ± 0.8	1.60 (da)	96	FhG-ISE (10/95)	SunPower back-contact[38]
InP	24.3 ± 1.2[d]	0.075 (da)	99	NREL (2/91)	NREL, Entech cover[39]
CIGS (thin film)	21.5 ± 1.5[d]	0.102 (da)	14	NREL (2/01)	NREL
2-cell stacks					
GaAs/GaSb (4 terminal)	32.6 ± 1.7	0.053 (da)	100	Sandia[e] (10/89)	Boeing, mechanical stack[40]
InP/GaInAs (3 terminal)	31.8 ± 1.6[d]	0.063 (da)	50	NREL (8/90)	NREL, monolithic[41]
GaInP/GaInAs (2-terminal)	30.2 ± 1.2	0.1326 (da)	300	NREL/FhG-ISE (6/01)	Fraunhofer, monolithic[42]
GaInP/GaAs (2 terminal)	30.2 ± 1.4	0.103 (da)	180	Sandia (3/94)	NREL, monolithic[43]
GaAs/Si (large) (4-terminal)	29.6 ± 1.5[d]	0.317 (da)	350	Sandia[e] (9/88)	Varian/Stanford/ Sandia, mech. Stack[44]
3-cell stacks					
GaInP/GaAs/Ge (2-terminal)	34.7 ± 1.7	0.2665(da)	333	NREL (9/03)	Spectrolab, monolithic
Submodules					
GaInP/GaAs/Ge	27.0 ± 1.5	34 (ap)	10	NREL (5/00)	ENTECH[45]
GaAs/GaSb	25.1 ± 1.4	41.4 (ap)	57	Sandia (3/93)	Boeing, 3 mech. stack units[46]
Modules					
Si	20.3 ± 0.8[d]	1875 (ap)	80	Sandia (4/89)	Sandia/UNSW/ ENTECH (12 cells)[47]
Low-AOD spectrum[f]					
GaInP/GaInAs/Ge (2-terminal)	**39.0 ± 2.3[f]**	**0.2691 (da)**	**236**	**NREL (5/05)**	**Spectrolab, low-AOD spectrum[8]**
Si	27.6 ± 1.0	1.00 (da)	92	FhG-ISE (11/04)	Amonix back-contact[7]
'Notable exceptions'					
GaInP/GaInAs/Ge (2-terminal)	**38.8 ± 2.3[f]**	**0.254(da)**	**241**	**NREL (5/05)**	**Spectrolab, metamorphic[8]**
Si (large)	21.6 ± 0.7	20.0 (da)	11	Sandia[e] (9/90)	UNSW laser grooved[48]
GaAs (Si substrate)	21.3 ± 0.8	0.126 (da)	237	Sandia (5/91)	Spire[37]
InP (GaAs substrate)	21.0 ± 1.1[d]	0.075 (da)	88	NREL (2/91)	NREL, Entech cover[49]

[a] Effic. = efficiency.

[b] (da) = designated illumination area; (ap) = aperture area.

[c] One sun corresponds to an intensity of 1000 Wm^{-2}.

[d] Not measured at an external laboratory.

[e] Measurements corrected from originally measured values due to Sandia recalibration in January, 1991.

[f] Low aerosol optical depth direct beam AM1.5 spectrum.

Schematic of operation of the dye-sensitized electrochemical photovoltaic cell

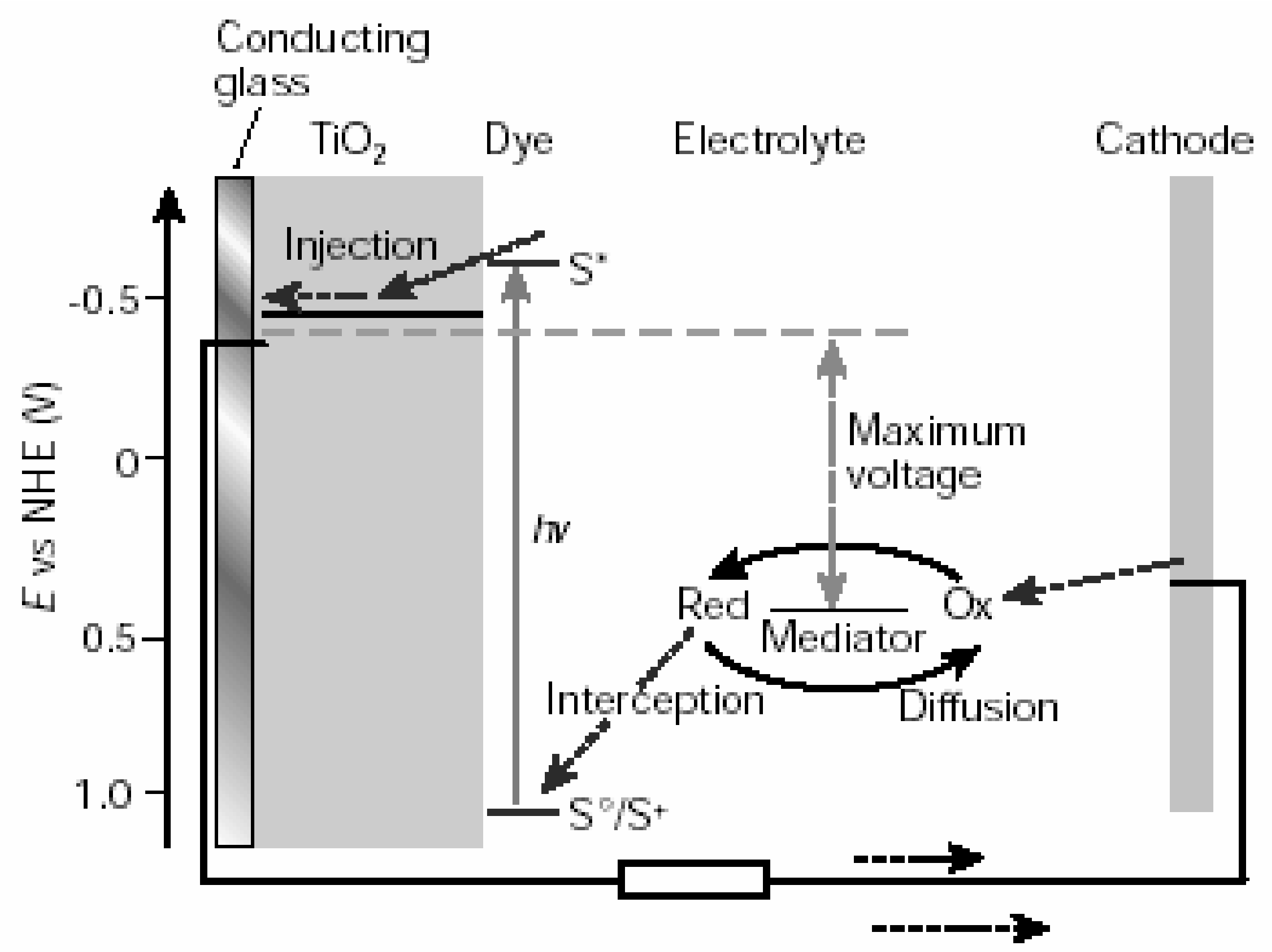

Nanocrystalline TiO_2 dye-sensitised solar cell

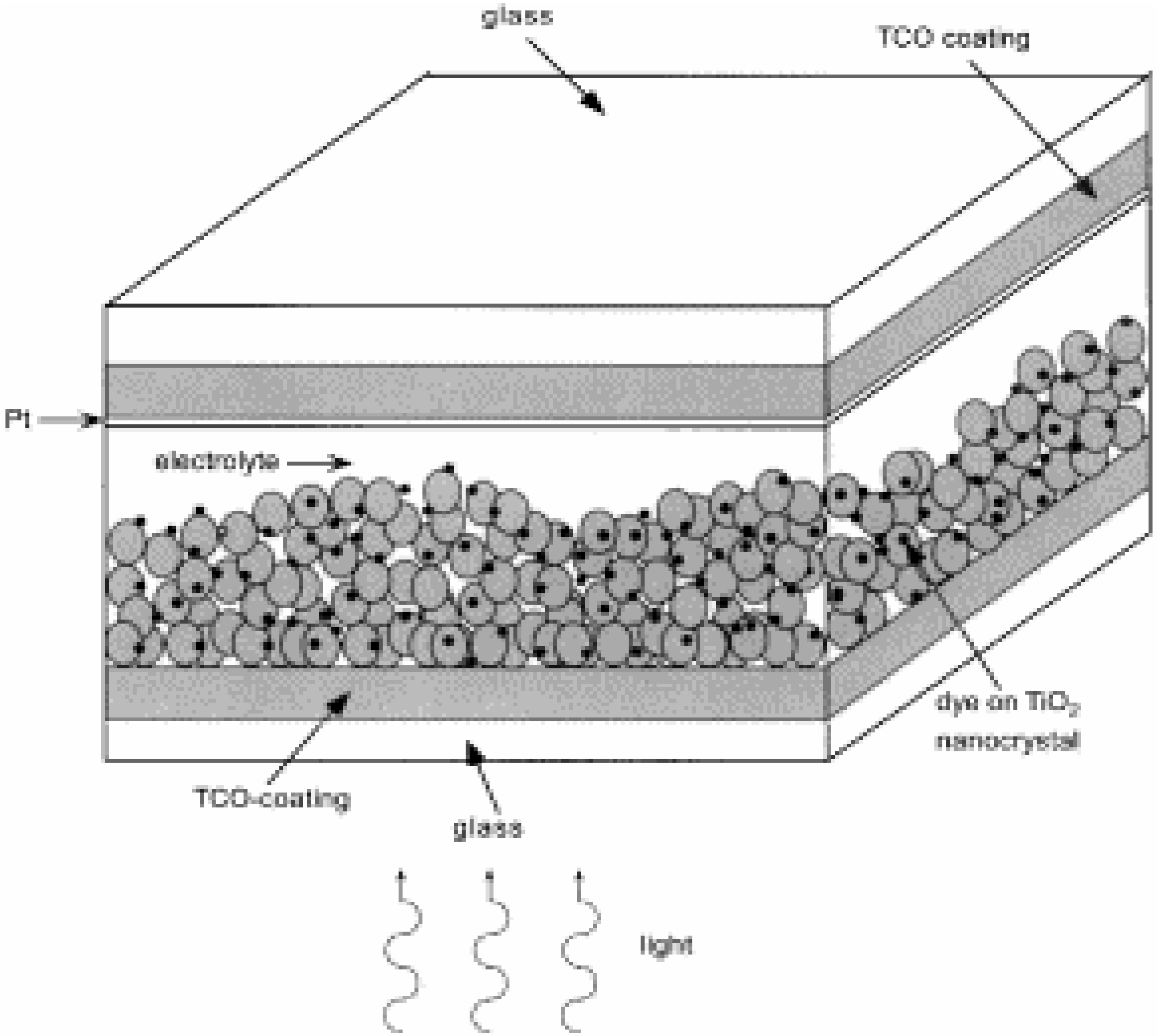

Scanning electron micrograph of the surface of a mesoporous anatase film prepared from a hydrothermally processed TiO_2 colloid. The exposed surface planes have mainly {101} orientation

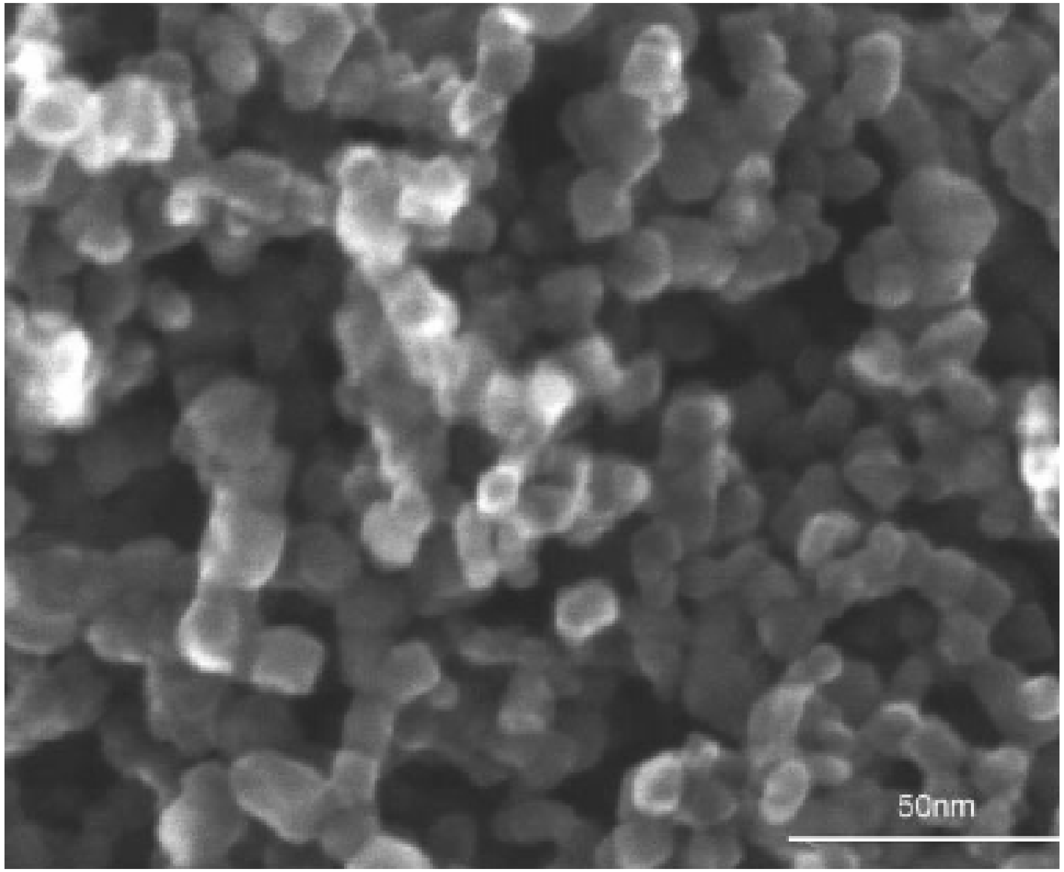

cis-RuL$_2$- (NCS)$_2$

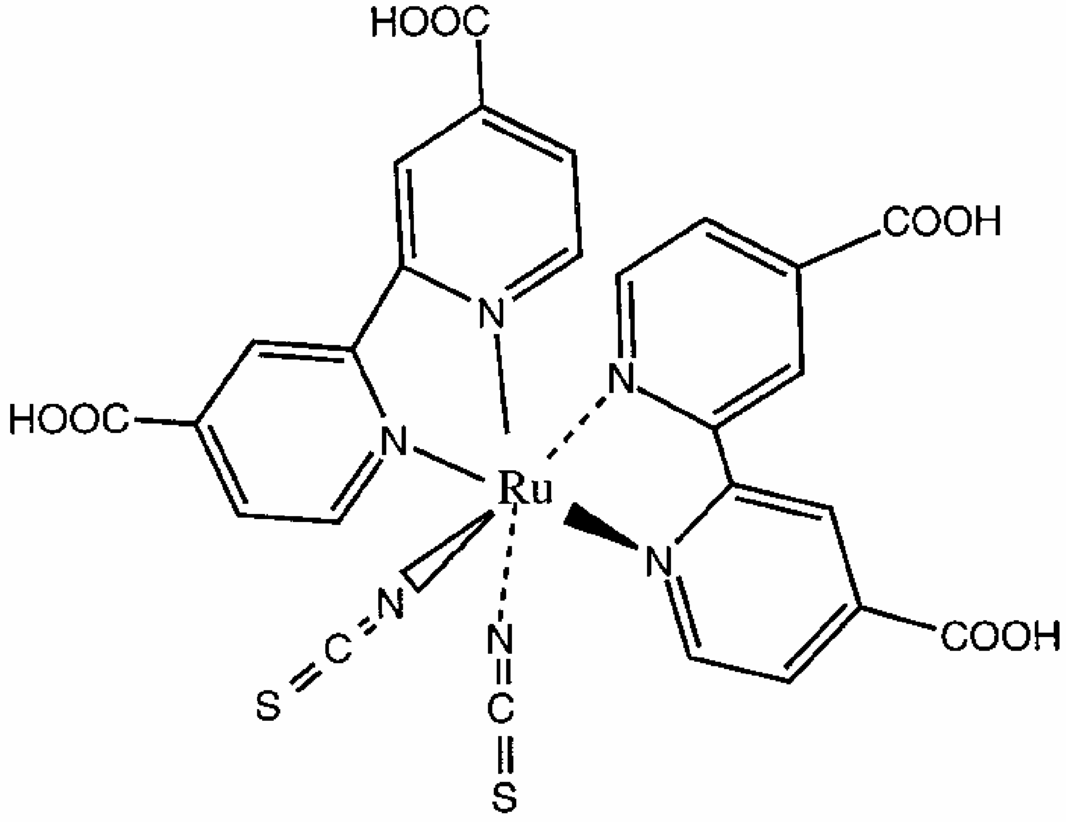

N3

Spectral response curve of the photocurrent for the DYSC sensitized by N3 and the black dye

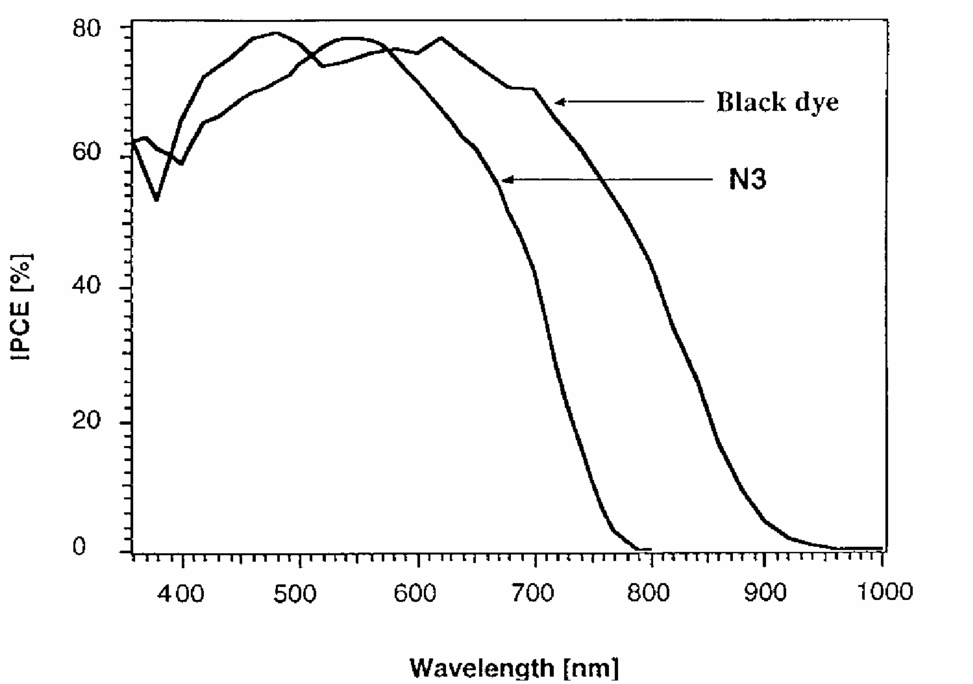

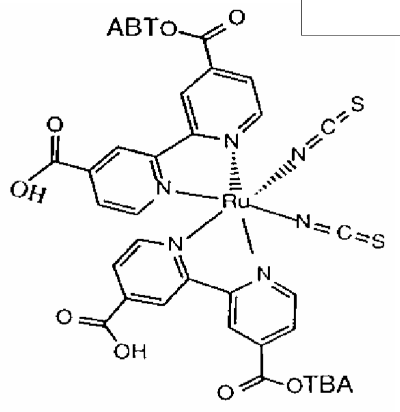

N3

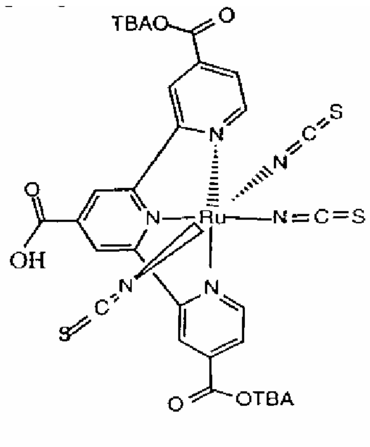

Black dye

Dynamics of redox processes involved in the conversion of light to electric power by dye-sensitized solar cells

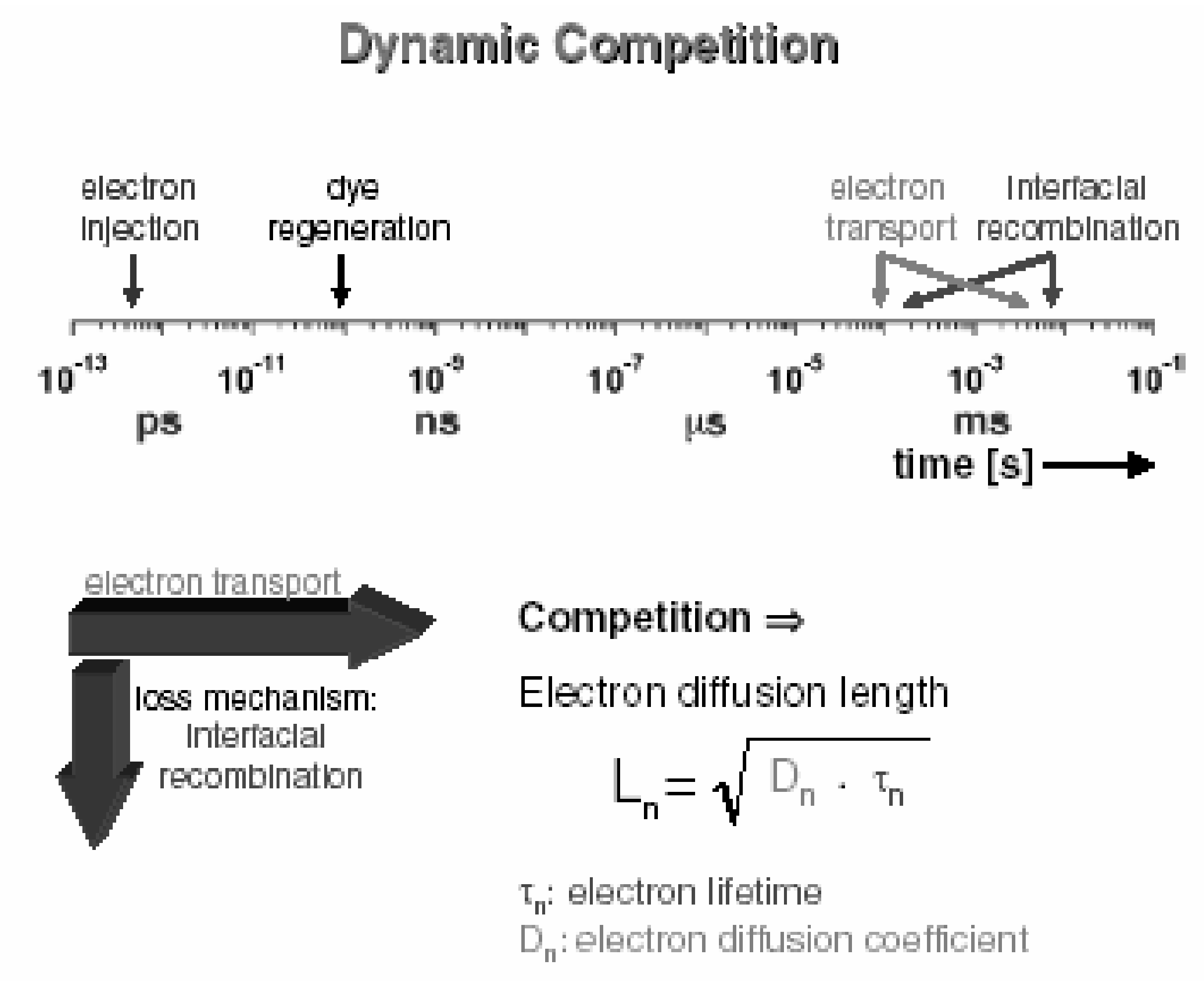

Competition ⇒

Electron diffusion length

$$L_n = \sqrt{D_n \cdot \tau_n}$$

τ_n: electron lifetime
D_n: electron diffusion coefficient

Photocurrent-voltage characteristic of a nanocrystalline photoelectrochemical cell sensitized with the panchromatic black dye.

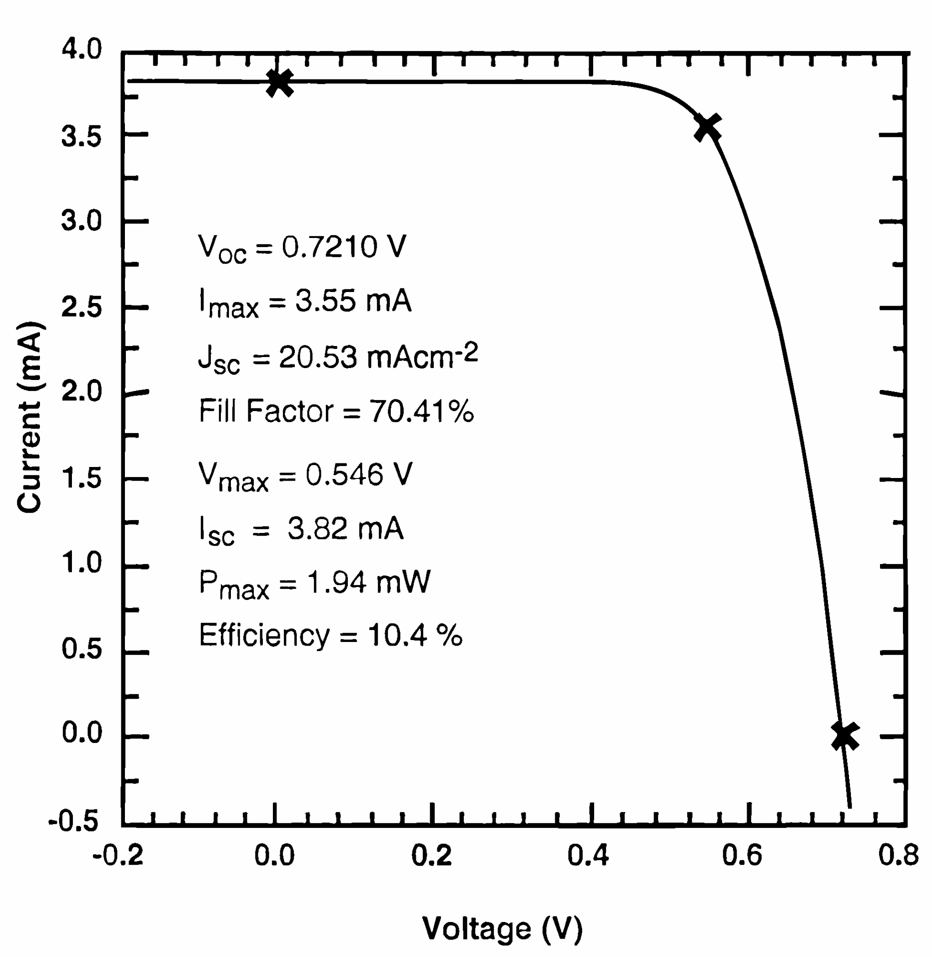

V_{oc} = 0.7210 V

I_{max} = 3.55 mA

J_{sc} = 20.53 $mAcm^{-2}$

Fill Factor = 70.41%

V_{max} = 0.546 V

I_{sc} = 3.82 mA

P_{max} = 1.94 mW

Efficiency = 10.4 %

Photocurrent voltage curves of a DSC at different light intensities

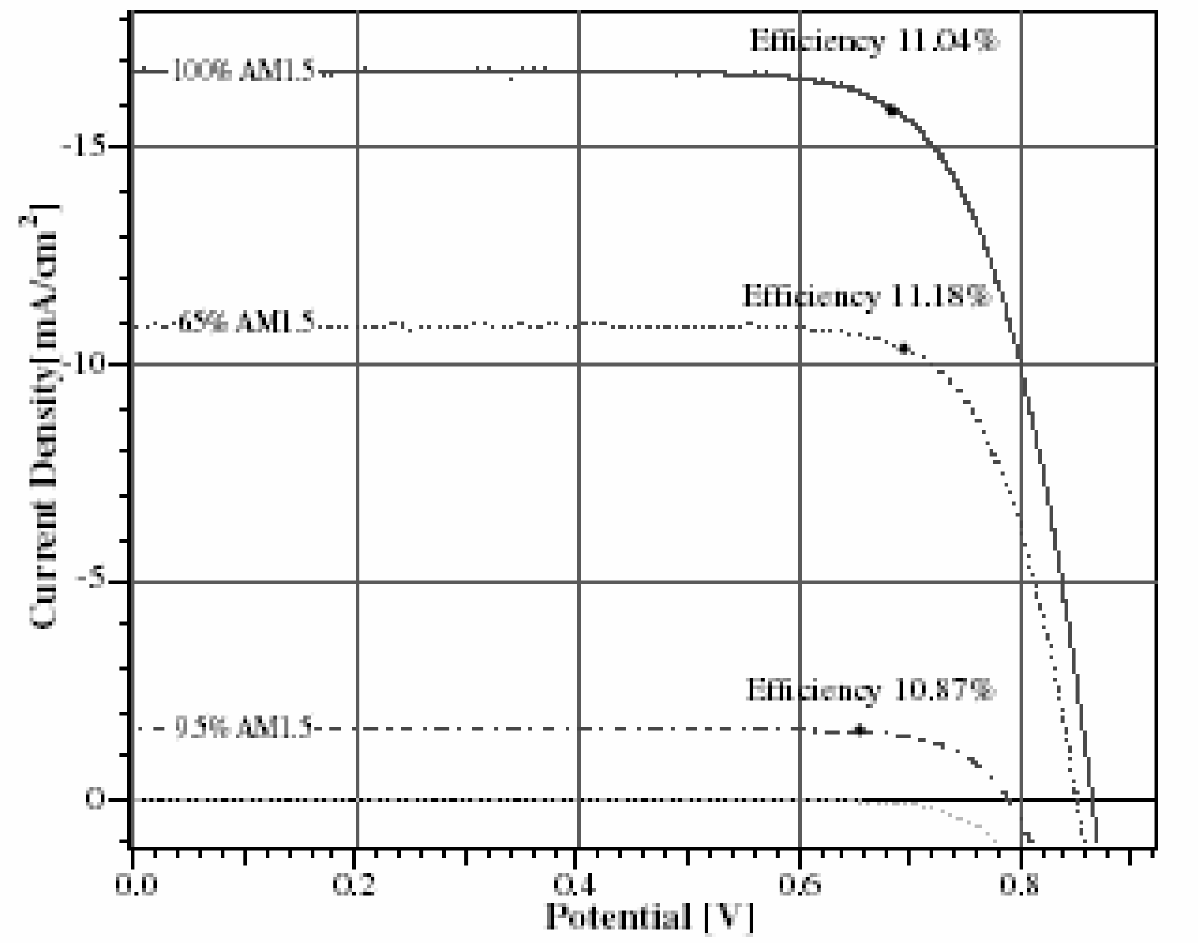

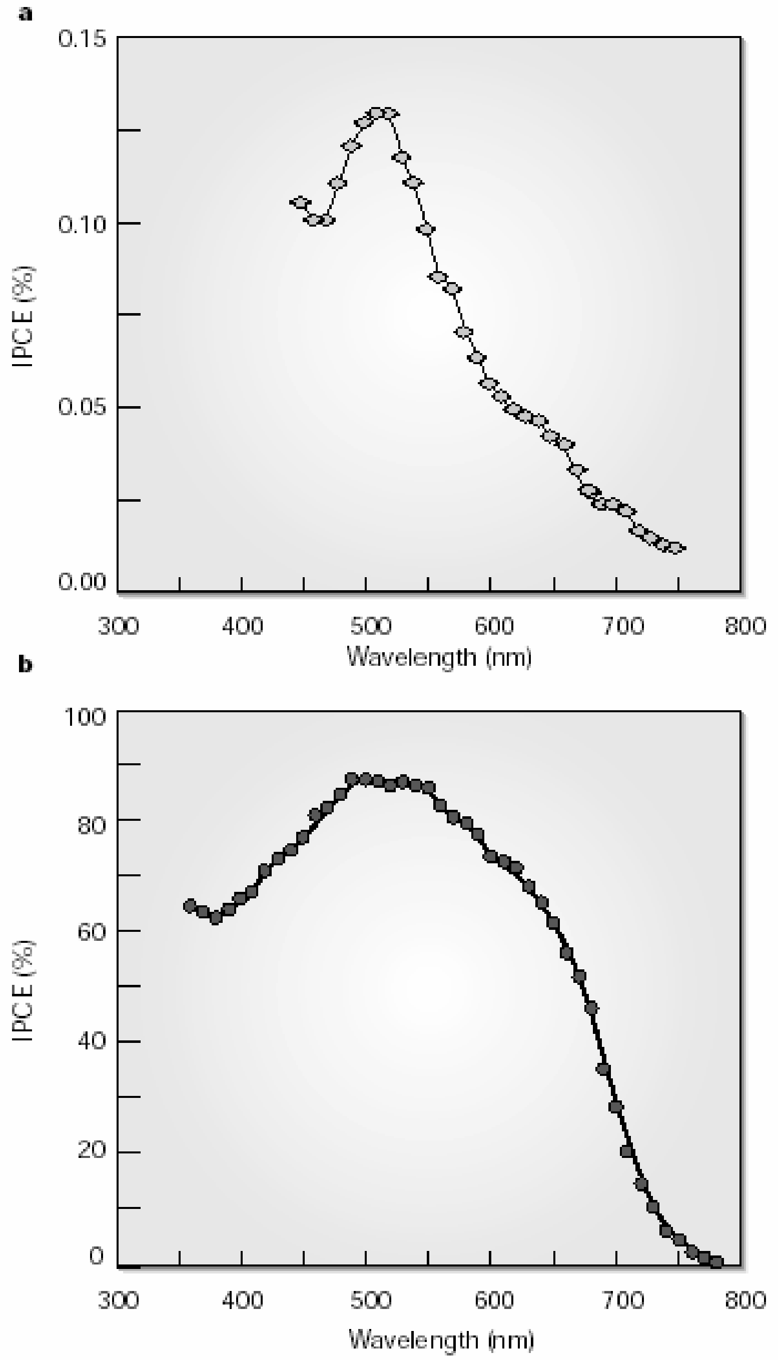

Conversion of light to electric current by dye-sensitized solar cells. The incident photon to current conversion efficiency is plotted as a function of the excitation wavelength. Top: single crystal anatase cut in the (101) direction. Bottom: nanocrystalline anatase film. The electrolyte consisted of a solution of 0.3M LiI and 0.03M I_2 in acetonitrile.

What is the exact role of the electrolyte penetrating the pores of a nanostructured TiO_2 electrode ?

A nanostructured TiO_2 film is to be viewed as a three-dimensional electrode of finite conductivity.

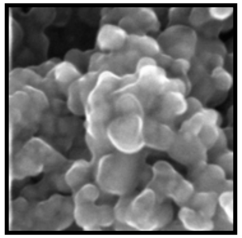

In a dye-sensitized TiO_2 photoanode the current enters through the outer photoanode/electrolyte interface as an ionic current, then starts to be gradually converted, via the photoinduced charge transfer reaction, into an electronic current within the TiO_2 matrix to finally reach the back contact as the solely electronic current*

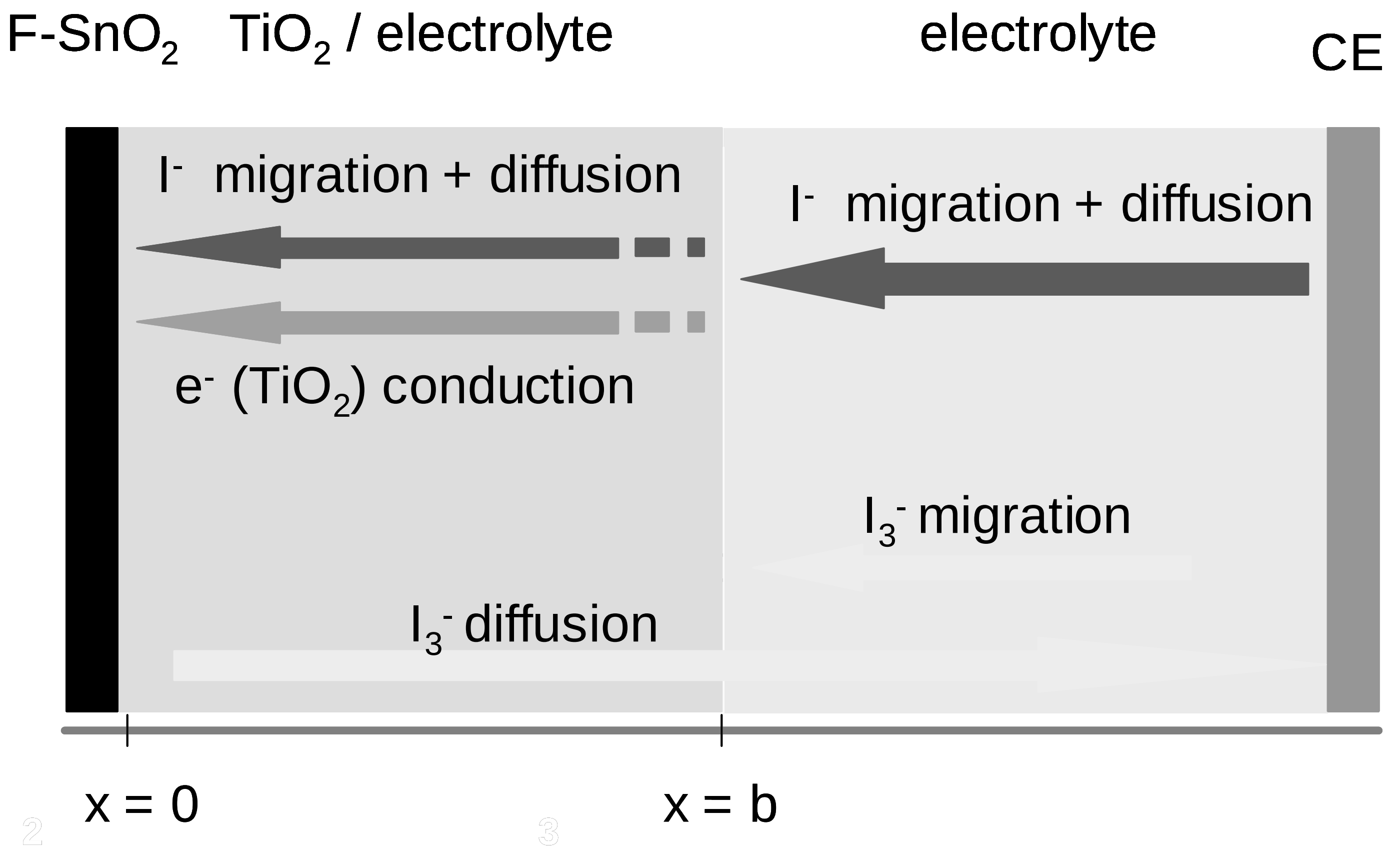

$$\mathbf{TiO_2/dye + h\nu + 3\ I^- \rightarrow I_3^- + 2e^-} \qquad \mathbf{I_3^- + 2e^- \rightarrow 3\ I^-}$$

Schematic representation of main ionic and electronic fluxes involved in the operation of the dye-sensitized liquid-junction photovoltaic cell, employing an electrolyte composed principally of an iodide salt (such as LiI), under steady-state conditions. To simplify the scheme, the drift of Li$^+$ cations is not shown.

In this regenerative cell a redox mediator, the I^- ion, is oxidized at the photoanode into I^-_3 which becomes reduced at the cathode. Due to the absence of the supporting electrolyte, the ionic current within the nanocrystalline TiO_2 photoanode is carried by the redox mediator I^- anion and its counter-ion, Li^+.

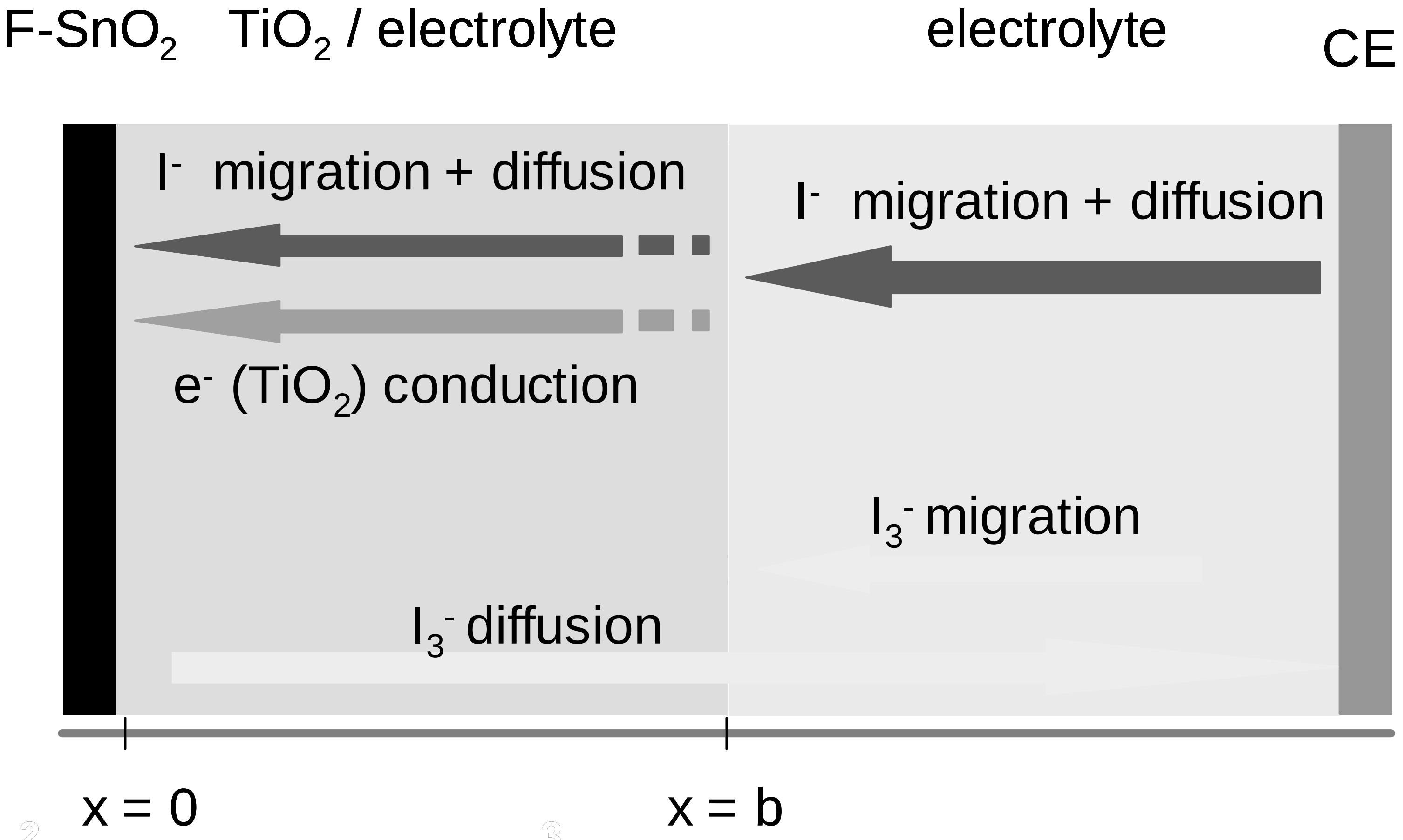

$F\text{-}SnO_2$ TiO_2 / electrolyte

electrolyte

CE

I^- migration + diffusion

I^- migration + diffusion

e^- (TiO_2) conduction

I_3^- migration

I_3^- diffusion

$x = 0$

$x = b$

The sequence of events occurring at the dye-sensitized TiO_2 photoanode can be summarized as follows:

$$\text{dye} + h\nu \rightarrow \text{dye}^*$$

$$\text{dye}^* \rightarrow \text{dye}^+ + e^-_{\text{TiO2}}$$

$$\text{dye}^+ + I^- \rightarrow 0.5\ I_2$$

and $I_2 + I^- \rightarrow I^-_3$

The *overall reaction* occurring at the photoanode may be represented simply as:

$$TiO_2/\text{dye} + h\nu + I^- \rightarrow 0.5\ I_2 + e^-$$

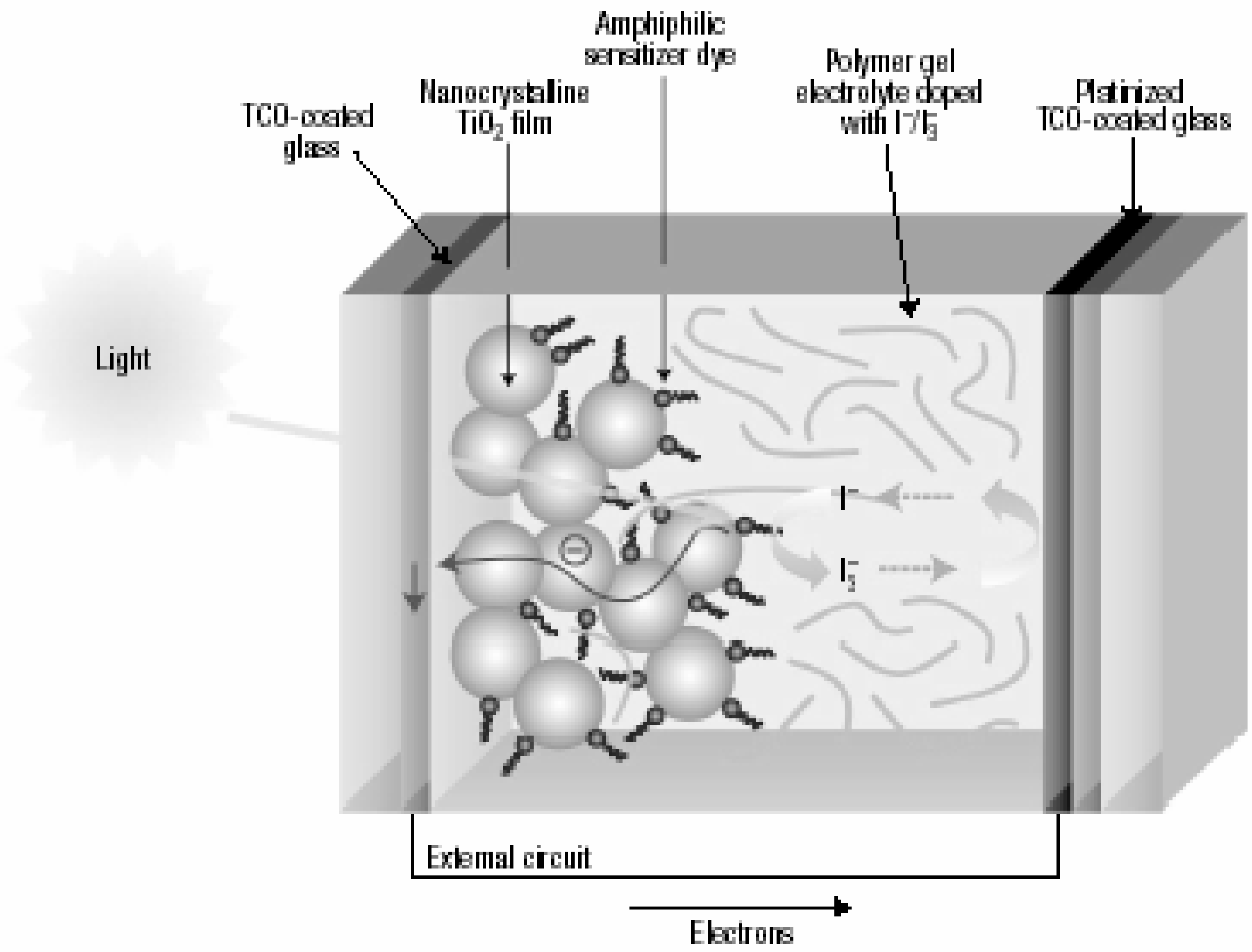

The design for optimal stability and efficiency in a dye-sensitized solar cell. The device is based on a novel composite film comprising a mesoporous, nanocrystalline TiO2 film (the grey spheres) sensitized by an amphiphilic ruthenium dye (the red molecules),with polymer gel electrolyte (brown lines) interpenetrated into the film pores.This system is sandwiched between two transparent conducting oxide (TCO) electrodes.